

# The ALMA Survey of 70 $\mu$ m Dark High-mass Clumps in Early Stages (ASHES). VI. The core-scale CO-depletion.

GIOVANNI SABATINI <sup>1</sup> STEFANO BOVINO <sup>1,2</sup> PATRICIO SANHUEZA <sup>3,4</sup> KAHU MORII <sup>3,5</sup> SHANGHUO LI <sup>6</sup>  
ELENA REDAELLI <sup>7</sup> QIZHOU ZHANG <sup>8</sup> XING LU <sup>9</sup> SIYI FENG <sup>10</sup> DANIEL TAFOYA <sup>11</sup> NATSUKO IZUMI <sup>12</sup>  
TAKESHI SAKAI <sup>13</sup> KEN'ICHI TATEMATSU <sup>4,14</sup> AND DAVID ALLINGHAM <sup>15</sup>

- <sup>1</sup>INAF - Istituto di Radioastronomia - Italian node of the ALMA Regional Centre (It-ARC), Via Gobetti 101, I-40129 Bologna, Italy  
<sup>2</sup>Departamento de Astronomía, Facultad Ciencias Físicas y Matemáticas, Universidad de Concepción, Av. Esteban Iturra s/n Barrio Universitario, Casilla 160, Concepción, Chile  
<sup>3</sup>National Astronomical Observatory of Japan, National Institutes of Natural Sciences, 2-21-1 Osawa, Mitaka, Tokyo 181-8588, Japan  
<sup>4</sup>Department of Astronomical Science, The Graduate University for Advanced Studies, SOKENDAI, 2-21-1 Osawa, Mitaka, Tokyo 181-8588, Japan  
<sup>5</sup>Department of Astronomy, Graduate School of Science, The University of Tokyo, 7-3-1 Hongo, Bunkyo-ku, Tokyo 113-0033, Japan  
<sup>6</sup>Korea Astronomy and Space Science Institute, 776 Daedeokdae-ro, Yuseong-gu, Daejeon 34055, Republic of Korea  
<sup>7</sup>Max-Planck-Institut für extraterrestrische Physik, Gießenbachstraße 1, D-85749 Garching bei München, Germany  
<sup>8</sup>Center for Astrophysics, Harvard & Smithsonian, 60 Garden Street, Cambridge, MA 02138, USA  
<sup>9</sup>Shanghai Astronomical Observatory, Chinese Academy of Sciences, 80 Nandan Road, Shanghai 200030, People's Republic of China  
<sup>10</sup>Department of Astronomy, Xiamen University, Zengcuo'an West Road, Xiamen, 361005 China  
<sup>11</sup>Department of Space, Earth and Environment, Chalmers University of Technology, Onsala Space Observatory, 439 92 Onsala, Sweden  
<sup>12</sup>Academia Sinica Institute of Astronomy and Astrophysics, No.1, Section 4, Roosevelt Road, Taipei 10617, Taiwan, Republic of China  
<sup>13</sup>Graduate School of Informatics and Engineering, The University of Electro-Communications, Chofu, Tokyo 182-8585, Japan.  
<sup>14</sup>Nobeyama Radio Observatory, National Astronomical Observatory of Japan, National Institutes of Natural Sciences, 462-2 Nobeyama, Minamimaki, Minamisaku, Nagano 384-1305, Japan  
<sup>15</sup>School of Mathematical and Physical Sciences, University of Newcastle, University Drive, Callaghan, NSW 2308, Australia

## ABSTRACT

Studying the physical and chemical properties of cold and dense molecular clouds is crucial for the understanding of how stars form. Under the typical conditions of infrared dark clouds, CO is removed from the gas phase and trapped on to the surface of dust grains by the so-called depletion process. This suggests that the CO depletion factor ( $f_D$ ) can be a useful chemical indicator for identifying cold and dense regions (i.e., prestellar cores). We have used the 1.3 mm continuum and C<sup>18</sup>O(2-1) data observed at the resolution of  $\sim 5000$  au in the ALMA Survey of 70  $\mu$ m Dark High-mass Clumps in Early Stages (ASHES) to construct averaged maps of  $f_D$  in twelve clumps to characterise the earliest stages of the high-mass star formation process. The average  $f_D$  determined for 277 of the 294 ASHES cores follows an unexpected increase from the prestellar to the protostellar stage. If we exclude the temperature effect due to the slight variations in the NH<sub>3</sub> kinetic temperature among different cores, we explain this result as a dependence primarily on the average gas density, which increases in cores where protostellar conditions prevail. This shows that  $f_D$  determined in high-mass star-forming regions at the core scale is insufficient to distinguish among prestellar and protostellar conditions for the individual cores, and should be complemented by information provided by additional tracers. However, we confirm that the clump-averaged  $f_D$  values correlates with the luminosity-to-mass ratio of each source, which is known to trace the evolution of the star formation process.

**Keywords:** Infrared dark clouds (787), Star-forming regions (1565), Star formation (1569), Massive stars (732), Interstellar medium (847), Astrochemistry (75), Interstellar line emission (844)

## 1. INTRODUCTION

Although high-mass stars ( $M > 8 - 10 M_\odot$ ) represent a small fraction compared to less massive counterparts, they play a major role in shaping the physical and chem-

ical properties of the interstellar medium (ISM). The formation of  $H_{II}$  regions at the end of the high-mass star formation process may favour conditions for triggering a secondary star formation cycle (Elmegreen 1998), involving molecular gas that is richer in complex organic molecules (COMs; Herbst & van Dishoeck 2009), a large number discovered in the hot molecular cores around massive young stellar objects (mYSO), e.g., Kurtz et al. (2000) and Cesaroni (2005). There is also evidence that the Sun was formed in a cluster that originally hosted high-mass stars (e.g., Adams 2010). Therefore, studying the details of the formation process of high-mass stars is crucial to understand how the chemical composition of the ISM evolves and how life arises from the organic materials produced during the star formation process.

In the last few decades, several theoretical scenarios have been proposed to describe the high-mass star formation process (e.g., Bonnell et al. 2001; McKee & Tan 2002; Tigé et al. 2017; Kumar et al. 2020; Padoan et al. 2020). These scenarios differ in the initial physical assumptions and predict different formation timescales. The identification and systematic study of the early stages of the high-mass star formation process, before the formation of mYSO(s), is hence crucial for distinguishing between the many existing scenarios (e.g., Zhang et al. 2009; Zhang & Wang 2011; Wang et al. 2014; Sanhueza et al. 2017, 2019).

Infrared dark clouds (IRDCs), originally identified in absorption against the galactic background in the mid-infrared (IR) at  $8\ \mu\text{m}$  (e.g., Perault et al. 1996; Egan et al. 1998), are so far considered the most likely birthplaces of high-mass stars. These are ubiquitous and extended ( $>10\ \text{pc}$ ) filamentary structures throughout the Galactic disc, which fragment into clumps and cores, with typical sizes of  $\sim 1\ \text{pc}$  and  $\lesssim 0.1\ \text{pc}$ , respectively (e.g., Carey et al. 1998; Rathborne et al. 2006; Simon et al. 2006a,b; Battersby et al. 2010; Peretto et al. 2016; Pokhrel et al. 2018; Li et al. 2022). By combining the IR and radio continuum properties obtained from several galactic plane surveys (e.g., MSX, Price et al. 2001; MIPS GAL, Carey et al. 2009; RMS, Urquhart et al. 2009; ATLAS GAL, Schuller et al. 2009; Hi-GAL, Molinari et al. 2010; CORNISH, Hoare et al. 2012)<sup>1</sup>, clumps can be classified into evolutionary stages.

As originally reported by Saraceno et al. (1996) for the low-mass regime, the high-mass clumps belonging to different phases also lie in different regions of the  $L$ - $M$  diagram (see Molinari et al. 2008), which compares the circumstellar envelope mass ( $M$ ) and the bolometric luminosity ( $L$ ) for a given clump. The luminosity-to-mass ratio ( $L/M$ ) of the clumps increases from the prestellar- to the more evolved  $H_{II}$ -stage as a signature of forming mYSOs, and has therefore been used as an additional diagnostic tool to identify clumps at different evolutionary stages (e.g., Molinari et al. 2008; Elia et al. 2017; Giannetti et al. 2017a; Urquhart et al. 2018, 2022; Sabatini et al. 2021). According to this general scheme, clumps that lack 24 and  $70\ \mu\text{m}$  emission also show a lower  $L/M$  ratio and are usually associated with the quiescent/prestellar-stage (e.g., Zhang et al. 2014; Chambers et al. 2009; Sanhueza et al. 2012, 2013, 2019; Guzmán et al. 2015). However, even under these conditions, it is not possible to completely rule out the presence of star-forming activity in these clumps, which can reveal the presence of cores at different evolutionary stages when observed at high resolution (e.g., Feng et al. 2016b; Sanhueza et al. 2019; Li et al. 2019, 2020; Morii et al. 2021; Tafuya et al. 2021; Sakai et al. 2022).

Additional chemical constraints have been proposed over time to better characterise the evolutionary picture of the high-mass star formation process. Under the typical physical conditions of dense regions in IRDCs,  $n(\text{H}_2) \gtrsim 10^4\ \text{cm}^{-3}$  and  $T_{\text{gas}} \lesssim 20\ \text{K}$ , a well-known example of chemical constraint is given by the estimates of the CO depletion (e.g., Kramer et al. 1999; Bergin et al. 2002; Caselli et al. 2008; Wiles et al. 2016; Sabatini et al. 2019; Feng et al. 2020), that has been used in particular to identify the youngest clumps (e.g., Fontani et al. 2006; Pillai et al. 2007; Giannetti et al. 2014).

How much of CO is depleting on to the surface of dust grains is usually characterised by the depletion factor (e.g., Caselli et al. 1999; Fontani et al. 2012; Sabatini et al. 2019), defined as the ratio between the expected CO/ $\text{H}_2$  abundance ( $X_{\text{CO}}^{\text{E}}$ ) and the observed one ( $X_{\text{CO}}^{\text{O}}$ ):

$$f_{\text{D}} = \frac{X_{\text{CO}}^{\text{E}}}{X_{\text{CO}}^{\text{O}}} = \frac{X_{\text{CO}}^{\text{E}} N(\text{H}_2)}{N(\text{CO})}, \quad (1)$$

where  $N(\text{H}_2)$  and  $N(\text{CO})$  are the  $\text{H}_2$  and CO column density, respectively. CO-depletion factors of up to a few tens have been derived on clump-scale in various samples of young, high-mass star-forming regions (e.g., Thomas & Fuller 2008; Fontani et al. 2012; Feng et al. 2016a, 2020). The estimation of  $f_{\text{D}}$  could be a suitable and convenient way to identify the cold/prestellar gas also at core-scales. However, very few and isolated estimates of  $f_{\text{D}}$  on these scales are found in the literature in

<sup>1</sup> ATLAS GAL: The Atacama Pathfinder EXperiment (APEX, Güsten et al. 2006) Telescope Large Area Survey of the Galaxy; CORNISH: The Coordinated Radio and Infrared Survey for High-Mass Star Formation; Hi-GAL: Herschel (Pilbratt et al. 2010) InfraRed Galactic Plane Survey; MIPS GAL: Multiband Imaging Photometer (MIPS, Rieke et al. 2004) Galactic Plane Survey; MSX: Midcourse Space Experiment Survey of the Galactic Plane; RMS: The Red MSX Source Survey;

**Table 1.** Summary of the physical and chemical properties of the ASHES sources.

Clump-ID	$d_{\odot}^a$	$R_{GC}^a$	$Mass^b$	$R_{eff}^c$	$rms \text{ (mJy beam}^{-1})^d$		$(V_{lsr}^{C^{18}O})^e$	$(\sigma^{C^{18}O})^e$	$\gamma^f$	$(X_{C^{18}O}^E)^g$	$f_D^h$
	(kpc)	(kpc)	( $M_{\odot}$ )	( $''$ )	1.3 mm	$C^{18}O$ (2-1)	( $km \text{ s}^{-1}$ )	( $km \text{ s}^{-1}$ )			
(1)	(2)	(3)	(4)	(5)	(6)	(7)	(8)	(9)	(10)	(11)	(12)
G010.991–00.082	3.7	4.91	2230	27	0.115	5.150	$29.5 \pm 0.3$	$0.7 \pm 0.3$	74	$5.5 \times 10^{-7}$	2.8
G014.492–00.139	3.9	4.79	5200	23	0.168	5.200	$41.2 \pm 0.2$	$0.8 \pm 0.2$	72	$5.7 \times 10^{-7}$	4.6
G028.273–00.167	5.1	4.73	1520	24	0.164	5.310	$80.2 \pm 0.2$	$0.8 \pm 0.2$	71	$5.9 \times 10^{-7}$	3.5
G327.116–00.294	3.9	5.63	580	20	0.089	4.150	$-58.8 \pm 0.2$	$0.7 \pm 0.2$	85	$4.3 \times 10^{-7}$	1.9
G331.372–00.116	5.4	4.56	1640	24	0.083	4.270	$-87.8 \pm 0.1$	$0.6 \pm 0.1$	69	$6.3 \times 10^{-7}$	1.6
G332.969–00.029	4.4	5.03	730	28	0.080	4.320	$-66.5 \pm 0.2$	$0.7 \pm 0.2$	75	$5.3 \times 10^{-7}$	1.2
G337.541–00.082	4.0	5.08	1180	22	0.068	3.220	$-54.6 \pm 0.1$	$0.6 \pm 0.1$	76	$5.2 \times 10^{-7}$	2.1
G340.179–00.242	4.1	4.87	1470	37	0.094	5.190	$-51.8 \pm 0.2$	$0.8 \pm 0.2$	73	$5.6 \times 10^{-7}$	1.1
G340.222–00.167	4.0	4.96	760	19	0.112	5.490	$-51.7 \pm 0.1$	$0.7 \pm 0.1$	74	$5.4 \times 10^{-7}$	1.2
G340.232–00.146	3.9	4.98	710	25	0.139	5.440	$-50.5 \pm 0.1$	$0.8 \pm 0.1$	75	$5.3 \times 10^{-7}$	1.7
G341.039–00.114	3.6	5.23	1070	27	0.070	3.340	$-43.4 \pm 0.1$	$0.7 \pm 0.1$	79	$4.9 \times 10^{-7}$	1.1
G343.489–00.416	2.9	5.75	810	29	0.068	3.480	$-28.6 \pm 0.1$	$0.5 \pm 0.1$	87	$4.1 \times 10^{-7}$	1.9

NOTE—<sup>(a)</sup> Taken from Whitaker et al. (2017); <sup>(b)</sup> Derived from the Millimetre Astronomy Legacy Team 90 GHz (MALT90) Survey Contreras et al. (2017); <sup>(c)</sup> The clump’s effective radius was derived in Sanhueza et al. (2019) from Gaussian fitting to the ATLASGAL dust continuum emission at 870  $\mu m$ ; <sup>(d)</sup> The rms of dust continuum emission at 1.3 mm are taken from Sanhueza et al. (2019), while those of  $C^{18}O$  are computed from the data-cubes presented in Sect. 2; <sup>(e)</sup> Median local standard of rest velocities ( $V_{lsr}^{C^{18}O}$ ) and the velocity dispersions ( $\sigma^{C^{18}O}$ ) obtained from the  $C^{18}O$  (2-1) employing the Python Spectroscopic Toolkit (PySpecKit; Ginsburg & Mirocha 2011; Ginsburg et al. 2022; see also Appendix A); <sup>(f)</sup> Gas-to-dust ratio derived using Equation (3) (see Sect. 3.1); <sup>(g)</sup> Expected  $C^{18}O/H_2$  abundance derived using Equation (6) (see Sect. 3.3); <sup>(h)</sup> Average  $f_D$  of each clump determined following the procedure discussed in Sect. 4;

high-mass star-forming regions, with extreme values of  $f_D$  up to 100-1000 (Zhang et al. 2009; Morii et al. 2021; Rodríguez et al. 2021). In the absence of additional evidence for the high-mass regime, in this study we aim to test whether the CO-depletion factor can be considered a reliable tracer for cores at different evolutionary stages, embedded in high-mass star-forming regions.

This work is structured as follows: in Section 2 we describe the sample and the dataset on which this study is based; in Section 3 we report on the derivation of the maps of  $N(H_2)$  and  $C^{18}O$  used to construct the final  $f_D$  maps. In Section 4 we discuss the variation in the averaged  $f_D$  obtained for a population of cores at different evolutionary stages; finally, in Section 5 we summarise our conclusions.

## 2. SAMPLE AND DATA REDUCTION

The ALMA<sup>2</sup> Survey of 70  $\mu m$  Dark High-mass Clumps in Early Stages (ASHES; Sanhueza et al. 2019) provides an ideal basis for detailed studies of the earliest stages of the high-mass star formation process. In a pilot study (Sanhueza et al. 2019), 12 massive 70  $\mu m$  dark clumps

were mosaicked with ALMA in the dust continuum at  $\sim 224$  GHz ( $\sim 1.2''$  resolution), and used to characterise clump fragmentation (Table 1). We refer to Sanhueza et al. (2019) for a detailed description of the source selection criteria. From the dust continuum, a total of 294 cores were detected (excluding those located at the edges of the observed fields – i.e.,  $\sim 20$ -30% power point – where flux estimates are more uncertain)<sup>3</sup>. ASHES was designed to map the molecular emission of a large number of molecules in the ALMA Band-6, including CO,  $C^{18}O$ ,  $H_2CO$ ,  $CH_3OH$ , SiO,  $^{13}CS$ ,  $N_2D^+$ , DCN,  $DCO^+$ , and CCD. These tracers are used to characterise cores from a chemical point of view, allowing their classification into different evolutionary stages (see Li et al. 2020; Morii et al. 2021; Tafuya et al. 2021; Sakai et al. 2022; Li et al., 2022 in prep.).

Of the total population of 294 cores,  $\sim 71\%$  of cores (210 cores) are classified as prestellar, lacking of any star formation signatures, while  $\sim 29\%$  (84 cores) are classified as protostellar candidates, being associated with molecular outflows and/or “warm core” line emission

<sup>3</sup> The complete catalogue is available at <https://cdsarc.cds.unistra.fr/viz-bin/cat/J/ApJ/886/102>.

<sup>2</sup> The Atacama Large Millimeter/submillimeter Array (ALMA; Wootten & Thompson 2009).

(i.e.,  $\text{H}_2\text{CO}$  and  $\text{CH}_3\text{OH}$  lines with high upper energy levels).

Since different chemical conditions were assumed for the identification of the protostellar cores, they were additionally divided into three categories (Sanhueza et al. 2019; Li et al. 2020): (1) cores with molecular outflows (i.e., 24 cores, corresponding to  $\sim 8\%$  of the total population) identified via CO, SiO and/or  $\text{H}_2\text{CO}$  lines and in which no “warm cores” lines were detected; (2) “warm cores” (34 cores,  $\sim 12\%$ ) representing an evolutionary phase prior to the hot molecular core phase typically found to be associated with high-mass protostars. This class lacks in molecular outflow emission but shows a detection in one of the “warm cores” lines among  $\text{H}_2\text{CO}$   $J = 3_{2,2}-2_{2,1}$  ( $E_u/k_B = 68.09$  K; where  $k_B$  is the Boltzmann’s constant) and  $J = 3_{2,1}-2_{2,0}$  ( $E_u/k_B = 68.11$  K), and the  $\text{CH}_3\text{OH}$   $J_k = 4_{2,2}-3_{1,2}$  ( $E_u/k_B = 45.46$  K); (3) the remaining 26 cores (i.e., 9%) presumably belong to a more evolved protostellar stage with both molecular outflow and “warm cores” line detection.

So far, the ASHES project gives access to the largest population of prestellar cores candidate detected in high-mass star-forming clumps via a mix of dust continuum and line emission data, and reveals that even high-mass 70  $\mu\text{m}$  dark clumps can harbor a tiny fraction of deeply embedded cores with nascent star formation activity.

### 2.1. Observations

ALMA Band-6 observations were carried out in Cycles 3 and 4 (Project 2015.1.01539.S PI: P. Sanhueza) with the 12m-Array (Main Array, MA; Wootten & Thompson 2009) and the 7m-Array (Atacama Compact Array, ACA; Iguchi et al. 2009). Depending on the observed source, the 12m-array included 36-48 antennas distributed over baselines ranging between 15 and 700 m. The Atacama Compact Array includes 7-10 antennas, with baselines between 8 and 48 m. The average angular scales covered by these configurations range from a resolution  $\sim 1.25''$  to a maximum recoverable scale of  $\sim 19''$ . These scales correspond to spatial scales of  $\sim (5-70) \times 10^3$  au at the average distance of 4 kpc.

At the frequency of the  $\text{C}^{18}\text{O}(2-1)$  line,  $\nu_{2,1} \sim 219.5$  GHz, the typical  $1\sigma$  is 5 mJy beam $^{-1}$  (see Table 1), for a channel width of  $\sim 0.67$  km s $^{-1}$ . The data were calibrated with the Common Astronomy Software Applications (CASA) version 4.5.3, 4.6, and 4.7, while the CASA version 5.4 was employed for imaging. The  $\text{C}^{18}\text{O}$  cubes were produced using the automatic masking procedure *yclean* (Contreras et al. 2018). We refer to Sanhueza et al. (2019) for a more detailed description of the dataset.

## 3. ANALYSIS AND RESULTS

Based on Equation (1), the derivation of  $f_D$  requires the evaluation of the  $\text{H}_2$  and CO column densities. Since the main CO isotopologue (i.e.,  $^{12}\text{C}^{16}\text{O}$ ) is almost always optically thick (e.g., Heyer & Dame 2015), its intensity is not proportional to  $N(\text{CO})$ . Therefore, a less abundant CO isotopologue (i.e.,  $\text{C}^{18}\text{O}$ ) should be used to obtain a much more accurate estimate of  $f_D$ . In this Section, we summarise the procedure and the assumptions we follow to derive  $f_D$ .

### 3.1. $\text{H}_2$ column density maps

The beam-averaged  $\text{H}_2$  column density is computed in each pixel from the primary beam (PB) corrected ALMA continuum flux density at 1.3 mm,  $F_{1.3\text{ mm}}$ , as (e.g., Schuller et al. 2009)

$$N(\text{H}_2) = \frac{F_{1.3\text{ mm}} \gamma}{B_{1.3\text{ mm}}(T_{\text{dust}}) \Omega_{\text{app}} \kappa_{1.3\text{ mm}} \mu_{\text{H}_2} m_{\text{H}}}, \quad (2)$$

where  $B_{1.3\text{ mm}}(T_{\text{dust}})$  is the Planck function at 1.3 mm with a dust temperature  $T_{\text{dust}}$ ,  $\Omega_{\text{app}}$  is the beam solid angle<sup>4</sup>,  $\mu_{\text{H}_2} = 2.8$  is the  $\text{H}_2$  mean molecular weight (Kaufmann et al. 2008; see their Sect. A.1), and  $m_{\text{H}}$  is the mass of the hydrogen atom. We adopt a value of  $\kappa_{1.3\text{ mm}} = 0.9$  cm $^2$  g $^{-1}$ , which corresponds to the opacity of thin-icy-mantle dust grains at gas densities of  $10^6$  cm $^{-3}$  (Ossenkopf & Henning 1994).

In Equation (2) we assume  $T_{\text{dust}}$  equal to the  $\text{NH}_3$  kinetic temperature,  $T_{\text{kin}}^{\text{NH}_3}$ , derived from  $\text{NH}_3$  (1, 1) and (2, 2) transition lines obtained as part of the CACHMC survey (the Complete ATCA<sup>5</sup> Census of High-Mass Clumps; Allingham et al., 2022 in prep.) at  $\sim 5''$  angular resolution. Under typical conditions prevailing in IRDCs, the gas-dust thermal coupling is effective in regions where the gas density exceeds  $10^{4.5}$  cm $^{-3}$  (e.g., Goldsmith 2001). Overall, this density threshold is fulfilled in the entire population of cores identified in ASHES (e.g., Sanhueza et al. 2019, see also the additional discussion in Sect. 3.3). The methodology to derive the temperature from the  $\text{NH}_3$  observations is based on Mangum & Shirley (2015) and will be presented in a forthcoming paper describing the survey (Allingham et al., 2022 in prep.; see also Friesen et al. 2009; Hogge et al. 2018 and Keown et al. 2019). The temperature maps are finally regridded to the same pixel size as the ALMA maps. We mask the native temperature maps where the error is greater than 20% of the measured

<sup>4</sup> This is calculated assuming an equivalent radius for a circular beam with the same area as the ALMA beam.

<sup>5</sup> The Australia Telescope Compact Array (ATCA; e.g., Wilson et al. 2011).



$T_{\text{kin}}^{\text{NH}_3}$ , adopting for these pixels the median  $T_{\text{kin}}^{\text{NH}_3}$  temperature of all pixels with emission in the 1.3 mm dust continuum above  $3\sigma$  ( $\sigma$  obtained from Sanhueza et al. 2019; see Table 1). In each source the  $T_{\text{kin}}^{\text{NH}_3}$  ranges from  $\sim 7$  K to  $\sim 50$  K, showing on average mild temperature gradients that only in some rare cases reach a few tens Kelvin degrees within the same source. We find an average error of  $\sim 12\%$   $T_{\text{kin}}^{\text{NH}_3}$ , which corresponds to  $\sim 2$  K.

The gas-to-dust ratio,  $\gamma$ , is computed following Giannetti et al. (2017b) with a gradient of  $\gamma$  through the Galactic disc.

$$\log_{10}(\gamma) = 0.087 R_{\text{GC}} + 1.44, \quad (3)$$

where  $R_{\text{GC}}$  is the galactocentric distance of each source expressed in kpc (Table 1 and Whitaker et al. 2017). This prescription gives values of the gas-to-dust ratio between 69 and 87 (Table 1), and represents the second modification to the procedure followed by Sanhueza et al. (2019) to derive  $N(\text{H}_2)$ , where  $\gamma$  is taken to be 100. In the worst case scenario, this has produced a modest difference of 30% in the final  $N(\text{H}_2)$ , leaving however unchanged their gradient across the sources. This variation agrees with the intrinsic error of 32% derived in Sanhueza et al. (2017) considering the uncertainties associated with the dust opacity and  $\gamma$  in the mass determination of cores, and also reflects the typical error associated with  $N(\text{H}_2)$  considering the uncertainties on  $T_{\text{dust}}$  (e.g., Urquhart et al. 2018; Sanhueza et al. 2019). For this reason, we refer to Sanhueza et al. (2019), for the discussion on the distribution of  $N(\text{H}_2)$  in each source and for the visual inspection of the ALMA Band-6 continuum maps.

### 3.2. $\text{C}^{18}\text{O}$ column density maps

We derive the  $\text{C}^{18}\text{O}$  column density,  $N(\text{C}^{18}\text{O})$ , from its  $J = 2-1$  molecular transition observed with ALMA (see Sect. 2.1) by following Kramer & Winnewisser (1991)

$$N(\text{C}^{18}\text{O}) = \frac{3h C_\tau}{\eta_c 8\pi^3 \mu^2} f(T_{\text{ex}}^{\text{C}^{18}\text{O}}) \int T_{\text{b}} dv, \quad (4)$$

with,

$$f(T_{\text{ex}}^{\text{C}^{18}\text{O}}) = \frac{\mathcal{Z}}{2} \exp\left(\frac{E_1}{k_{\text{B}} T_{\text{ex}}}\right) \left[1 - \exp\left(-\frac{h\nu_{2,1}}{k_{\text{B}} T_{\text{ex}}}\right)\right]^{-1} \times [J(T_{\text{ex}}, \nu_{2,1}) - J(T_{\text{bg}}, \nu_{2,1})]^{-1}, \quad (5)$$

where  $h$  is the Planck constant, and  $\eta_c$  the beam filling factor assumed equal to 1. Also,  $\mu = 0.112 \times 10^{-18} \text{ dyn}^{0.5} \text{ cm}^2$  is the  $\text{C}^{18}\text{O}$  dipole moment,  $\mathcal{Z} = 0.36 T_{\text{ex}}^{\text{C}^{18}\text{O}} + 1/3$  is the partition function (e.g., Herzberg 1945),  $E_1$  is the energy of the lower level

of the transition,  $T_{\text{ex}}^{\text{C}^{18}\text{O}}$  is gas excitation temperature of  $\text{C}^{18}\text{O}$ ,  $J(T_{\text{ex}}, \nu) = (h\nu/k_{\text{B}})(\exp(h\nu/k_{\text{B}} T_{\text{ex}}) - 1)^{-1}$ ,  $T_{\text{bg}} = 2.7$  K the background temperature, and  $T_{\text{b}}$  the brightness temperature of the line. The integrated intensity is taken by considering the emission above the  $3\sigma$  threshold in a range of  $\pm 5 \text{ km s}^{-1}$  around the  $V_{\text{lsr}}$  reported in Table 1.

In Equation (4),  $f(T_{\text{ex}}^{\text{C}^{18}\text{O}})$  incorporates all the constants and the terms which depend on  $T_{\text{ex}}^{\text{C}^{18}\text{O}}$ . Also,  $C_\tau = \tau_{\text{C}^{18}\text{O}}/[1 - \exp(-\tau_{\text{C}^{18}\text{O}})]$  is the optical depth correction factor, valid for  $\tau \leq 2$  with uncertainty of about 15% (e.g., Frerking et al. 1982; Kramer & Winnewisser 1991), where  $\tau_{\text{C}^{18}\text{O}}$  is the optical depth of the  $\text{C}^{18}\text{O}(2-1)$  line derived following the approach discussed in Sabatini et al. (2019), and summarised in Appendix A. All the molecular parameters are taken from the Cologne Database for Molecular Spectroscopy (CDMS<sup>6</sup>; Müller et al. 2001). In each source, the  $1\sigma$  rms is computed as the average over five channels – far from the  $\text{C}^{18}\text{O}(2-1)$  line – of the flux’ standard deviations computed in a large region centred at the position of the source. We solve Equation (4) under the assumption of local thermodynamic equilibrium (LTE), i.e.,  $T_{\text{kin}}^{\text{NH}_3} = T_{\text{dust}} = T_{\text{ex}}^{\text{C}^{18}\text{O}}$ . The only exception is G332.969–00.029 that lacks in available  $\text{NH}_3$  data, and for which we assume  $T_{\text{dust}} = T_{\text{ex}}^{\text{C}^{18}\text{O}} = 12.6$  K, as the dust temperature reported by Guzmán et al. (2015). To avoid possible overestimates of  $N(\text{C}^{18}\text{O})$ , produced by too low  $T_{\text{ex}}^{\text{C}^{18}\text{O}} = T_{\text{kin}}^{\text{NH}_3}$  values, we impose a lower limit of  $T_{\text{ex}}^{\text{C}^{18}\text{O}} = 10.8$  K that corresponds to the separation between the levels of the  $\text{C}^{18}\text{O}(2-1)$  transition. In the worst-case scenario, this prescription affects less than 6% of the pixels where  $N(\text{C}^{18}\text{O})$  is computed. The opacity-corrected column density map of  $\text{C}^{18}\text{O}$ , also corrected for the primary beam effects, are shown in Appendix A. Our correction has increased  $N(\text{C}^{18}\text{O})$  by up to a factor of about  $\sim 1.8$ , producing  $N(\text{C}^{18}\text{O})$  spanning the range of  $\sim (0.1-6.4) \times 10^{16} \text{ cm}^{-2}$ .

### 3.3. Core-scale CO-depletion maps

The final CO-depletion factor maps, shown in Figures 1 and 2, are generated as the ratio between the expected and the observed abundance of CO relative to  $\text{H}_2$ , following Equation (1). For each source, we derive the expected  $\text{C}^{18}\text{O}/\text{H}_2$  abundance assuming (Frerking et al. 1982; Fontani et al. 2006; Giannetti et al. 2017b):

$$X_{\text{C}^{18}\text{O}}^{\text{E}} = \frac{9.5 \times 10^{-5} \times 10^{\alpha(R_{\text{GC}} - R_{\text{GC}, \odot})}}{^{16}\text{O}/^{18}\text{O}}, \quad (6)$$

<sup>6</sup> <https://cdms.astro.uni-koeln.de/cdms/portal/>

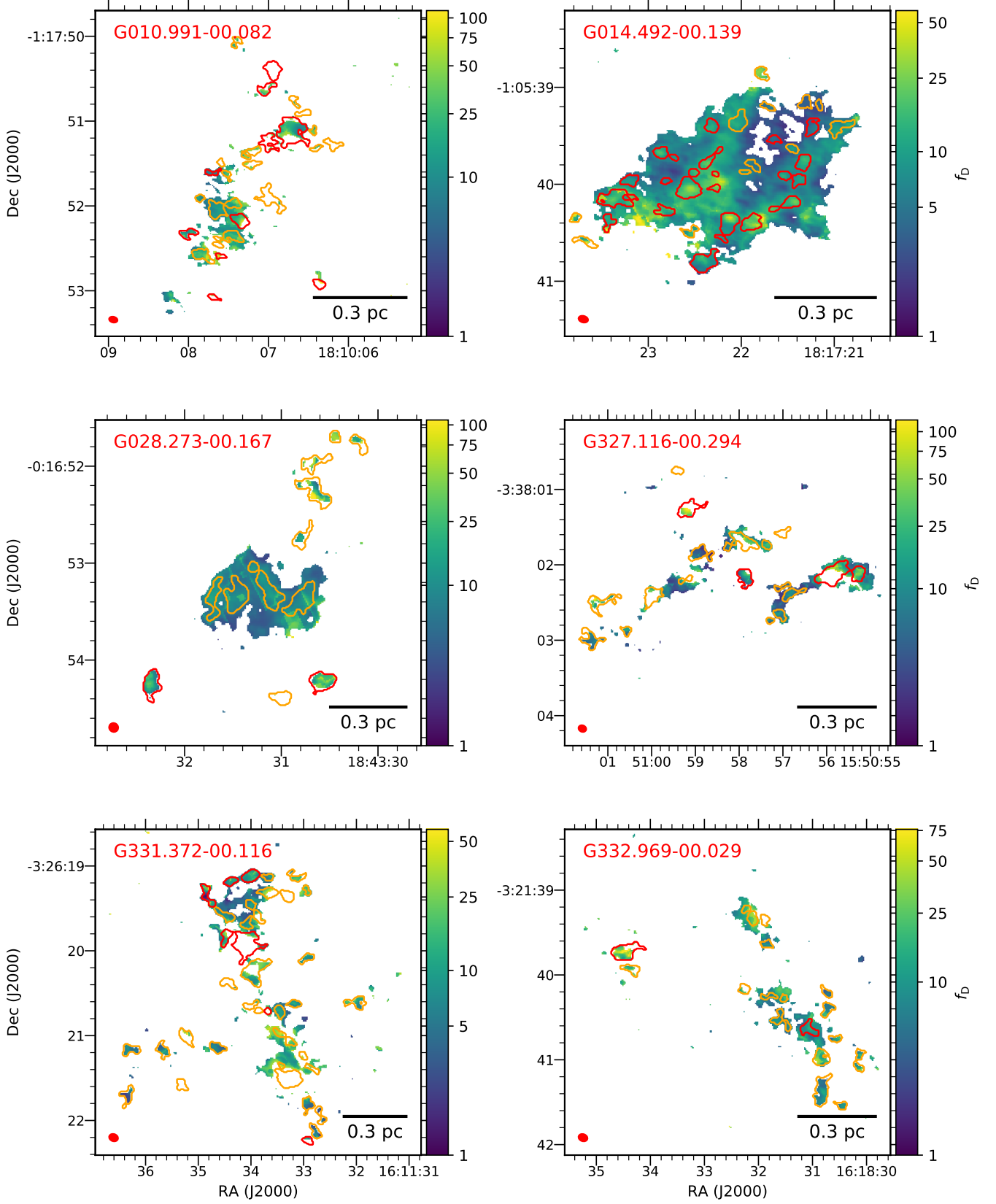


**Figure 1.** ASHES  $f_D$  maps obtained following the procedure explained in Sect. 3.3. The cores identified in Sanhueza et al. (2019) are shown as orange and red contours for prestellar and protostar cores, respectively, following the classification in Sect. 2.1. The ALMA synthesized beams are displayed in red at the bottom left in each panel, while the scalebar is shown in the bottom right corners. The color wedge of each panel displays the color scales corresponding to  $f_D$  in the log-scale.

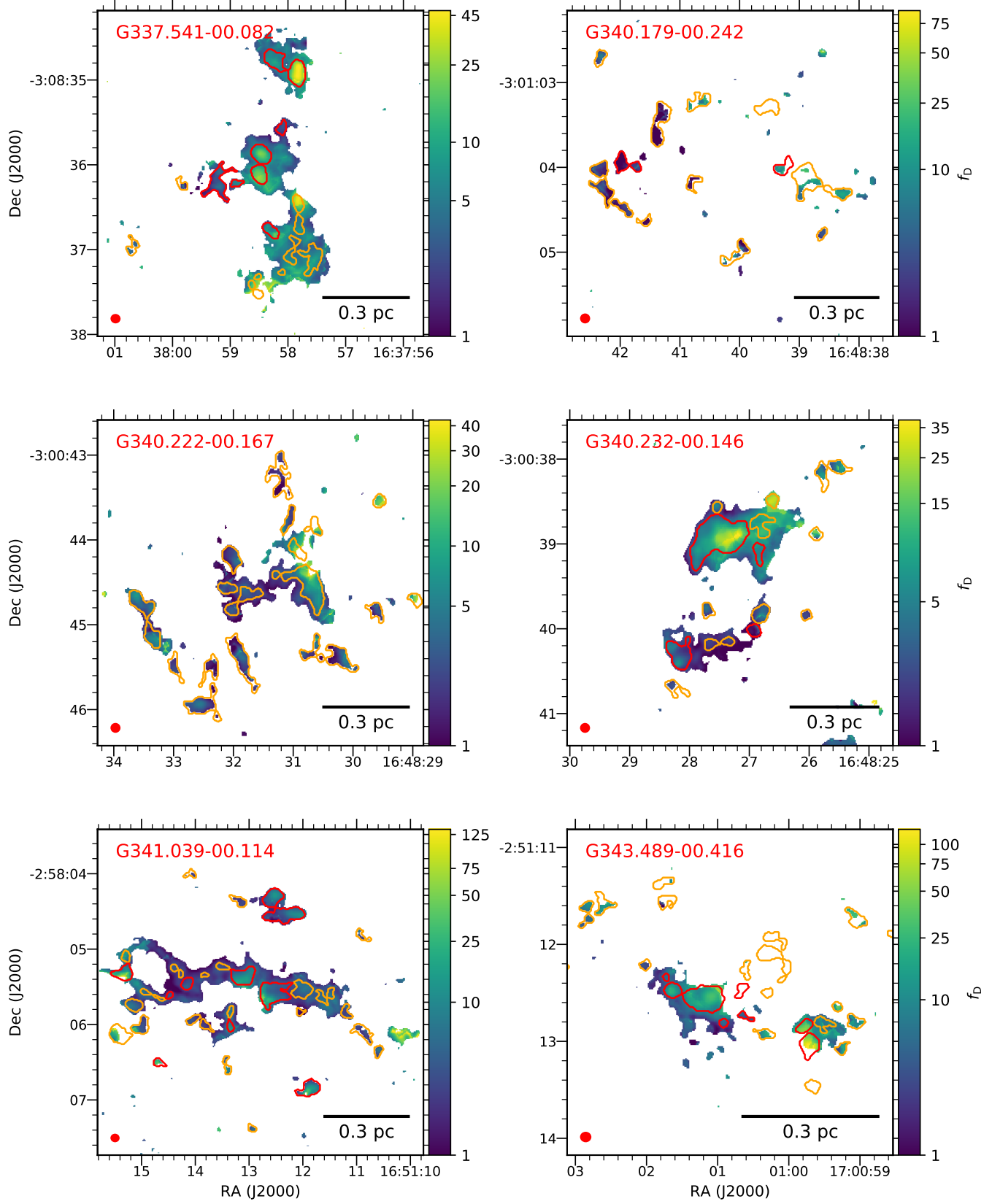
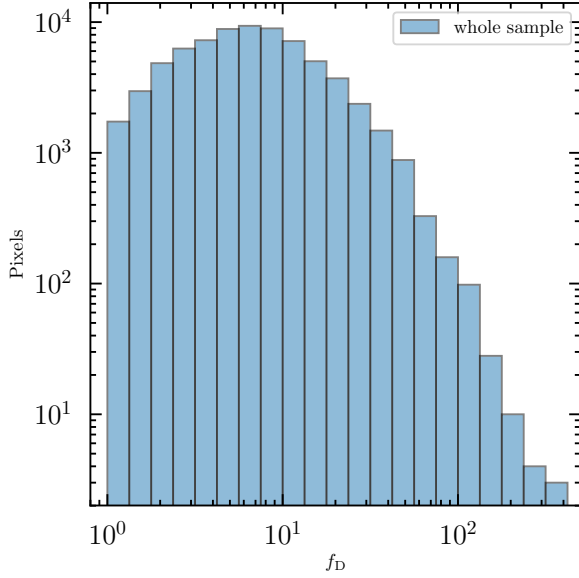


Figure 2. Continuation of Fig. 1.



**Figure 3.** Number distribution of  $f_D$  mapped in Figures 1 and 2. Pixel size is  $0.2''$ , while beam size is  $1.2''$ .

with  $R_{GC}$  expressed in kpc,  $R_{GC,\odot} = 8.34$  kpc (Reid et al. 2014), and  $\alpha = -0.08$  dex kpc $^{-1}$  describes the C/H abundance (Luck & Lambert 2011), under the assumption that the C/H abundance controls the CO formation<sup>7</sup>. The oxygen isotopic ratio,  $^{16}\text{O}/^{18}\text{O} = 58.8R_{GC} + 37.1$ , is computed according to Wilson & Rood (1994). We employ the galactocentric distances of the sources reported by Whitaker et al. (2017), according to Sanhueza et al. (2019). We find  $X_{C^{18}\text{O}}^E$  between  $4.1 \times 10^{-7}$  and  $6.3 \times 10^{-7}$  (see Table 1).

In each  $f_D$  map (Figures 1 and 2) we also report as orange/red regions the cores identified in Sanhueza et al. (2019): orange for the pre-stellar stage and red for the protostellar one (see Sect. 2).

The degree of depletion reveals widely different chemical conditions within the individual clumps. It spans regions where CO adsorption is almost irrelevant, with observed abundances of  $\text{C}^{18}\text{O}$  as expected (i.e.,  $f_D = 1$ ), up to regions where only less than 1% of the expected CO is still present in the gas phase (i.e.,  $f_D > 100$ )<sup>8</sup>.

<sup>7</sup> Note that the C/H abundance is given in dex units, which introduces the term  $10^\alpha$  in Equation 6

<sup>8</sup> Note that some of the cores identified in dust continuum are not associated with a value of  $f_D$  (e.g., see G010.991-00.082 and G327.116-00.294 in Fig. 1). However around those peculiar regions we find  $f_D$  among the highest over the entire clump. Thus, we expect extremely low abundances of  $\text{C}^{18}\text{O}$  within those cores (therefore high  $f_D$ ), below the limit of detection accessible to our observations (Table 1).

**Table 2.** Averaged  $f_D$  computed for the whole core sample

Clump-ID	Core-ID <sup>a</sup>	$\langle f_D \rangle_{\text{core}}$
G010.991-00.082	ALMA1	23.7
G010.991-00.082	ALMA2	92.8
G010.991-00.082	ALMA3	31.9
G010.991-00.082	ALMA4	...
G010.991-00.082	ALMA5	30.9
G010.991-00.082	ALMA6	56.3
G010.991-00.082	ALMA7	11.9
G010.991-00.082	ALMA8	27.6

NOTE—<sup>(a)</sup> The classification of cores follows that defined in Sanhueza et al. (2019). This table is available in its entirety in machine-readable form.

This is clear from Figure 3 that shows the number distribution of the CO-depletion values over the entire sample. On average, in  $\sim 85\%$  of the area mapped in  $f_D$ , more than 50% of the expected CO has been removed from the gas phase (i.e.,  $f_D > 2$ ). This is particularly relevant for the regions within the identified cores (both pre- and proto-stellar).

In the twelve sources shown in Figures 1 and 2, the behaviour of  $f_D$  follows an unexpected increase as the evolution of the cores progresses, i.e., going from pre- to proto-stellar (see Table 2). As an example, G014.492-00.139 (Fig. 1), with a large population of protostellar cores (i.e., 25 protostellar vs 12 pre-stellar cores), shows CO depletion that is comparable (and in some cases higher than) to clumps dominated by pre-stellar cores (e.g., G028.273-00.167 and G340.222-00.167; Fig. 1 and 2, respectively). This can be explained by exploring the physical conditions in the clumps. Due to the absence of protostars and outflows that can heat the gas surrounding the cores, these young clumps reveal mild temperature gradients. Looking at the regions associated with a  $> 3\sigma$  continuum emission, G028.273-00.167 and G340.222-00.167 show a  $\Delta T_{\text{kin}}^{\text{NH}_3} \sim 1$  K, and  $\sim 3$  K, respectively. If we then neglect the effect of temperature on the desorption process, it is reasonable that the evolution of the averaged  $f_D$  is mainly density-driven. This is confirmed by the results reported in Fig. 4(a), which show the depletion factor as a function of both density and temperature. This result also seems independent of the heliocentric distance associated with each ASHES clump, as discussed in Appendix B. From the same figure we can also see a weak temperature-effect when keeping the density constant, due to the weak temperature gradients in the  $T_{\text{kin}}^{\text{NH}_3}$  maps (see also Fig. 4b).



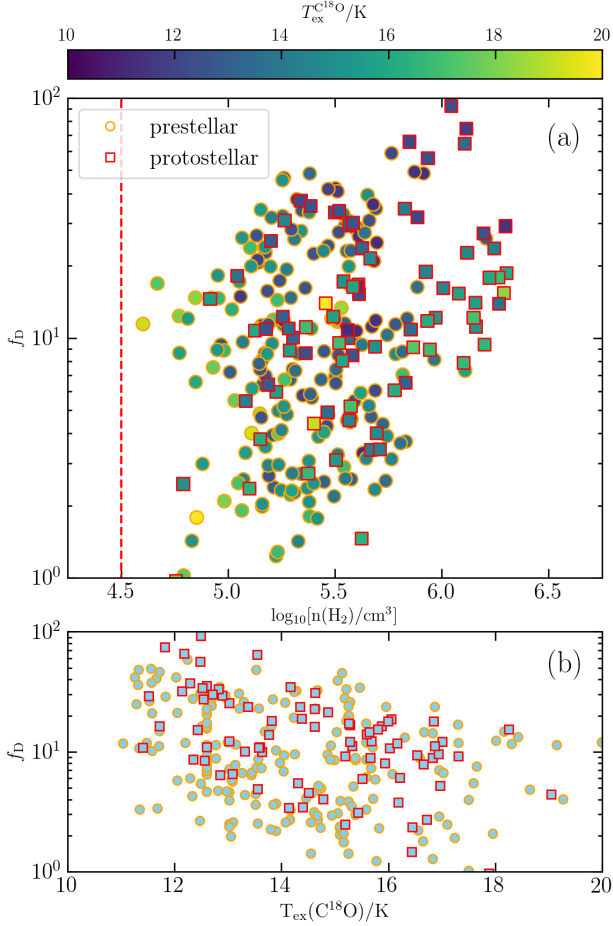


**Figure 4.** Panel (a): Scatter plot of the average properties of the cores identified in ASHES. The orange circles represent the prestellar cores, while the red squares refer to the cores classified as protostellar (Sect. 2). The red-dashed line represents the density threshold proposed by Goldsmith (2001) to ensure the gas-dust thermal coupling. Panel (b): Average  $f_D$  versus  $T_{\text{ex}}^{\text{C}^{18}\text{O}}$ . The gas excitation temperature of  $\text{C}^{18}\text{O}$  is assumed to be equal to the kinetic temperature of  $\text{NH}_3$ .

Within an evolutionary picture, clumps dominated by protostellar conditions, are characterized by densities on average larger than the pre-stellar ones (e.g., König et al. 2017; Elia et al. 2021 and Urquhart et al. 2022). The same evolutionary trend is also seen at cores-scale (Sanhueza et al. 2019). In addition, all the sources have been selected as 70  $\mu\text{m}$  dark and it is conceivable that the embedded protostars are at their early stages, i.e., yet to heat the surrounding gas significantly. It is then likely that the high degree of CO depletion is associated with the envelopes of these young protostellar objects, where protostellar activity has not yet led to a significant desorption of the frozen-out CO.

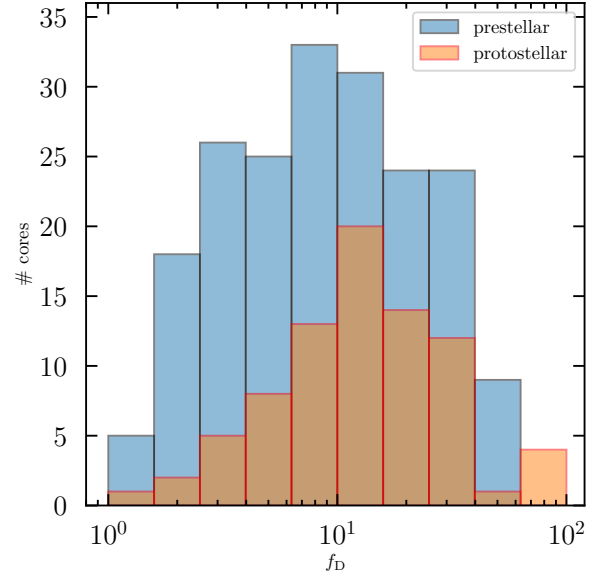


**Figure 5.** Number distributions of averaged  $f_D$  associated to each core identified in ASHES. The blue and orange histograms refer to prestellar and protostellar cores, respectively. A Kolmogorov-Smirnov two-sample test applied to the two distributions yields a  $p$ -value  $< 2 \times 10^{-3}$ .

In Fig. 5 we show the distributions of  $f_D$  for the entire population of pre- and proto-stellar cores in our sample; blue and orange histograms, respectively. The former show a median  $f_D$  of 8.5, while in the protostellar population we derive a median of 12.2. The protostellar distribution on average looks shifted towards higher values compared to the pre-stellar confirming what we observe in the maps, also in individual clumps (see Appendix B). This result is confirmed by a Kolmogorov-Smirnov (KS) test (Massey 1951). The test yields an  $p$ -value  $< 2 \times 10^{-3}$ , which is lower than the statistical significance level of 5% usually adopted to reject the hypothesis that the two datasets come from the same continuous distribution (e.g., Teegavarapu 2019).

#### 4. DISCUSSION

The study of CO-depletion in high-mass star-forming regions has been pursued over the years at different scales both via observations and theoretical studies. For example, the global distribution of  $f_D$  reported in Figures 1 and 2 is in agreement with the most recent state-of-the-art three-dimensional numerical simulations presented by Bovino et al. (2019), where the authors have simulated the collapse of turbulent and magnetized isothermal cores, exploring different initial conditions. They reported  $f_D$  values between 50-100 on a scale of 2000 au ( $\sim$  the effective radius associated with many of the cores identified in ASHES; Sanhueza et al. 2019),

qualitatively in line with our ALMA data. Notably, the values reported by [Bovino et al. \(2019\)](#) have been convolved with an ALMA-like point-spread function, showing a loss in the final  $f_D$  of a factor up to three when compared to the original simulated cubes. This might suggest the presence of compact regions where the chemistry of the CO is dramatically influenced by extreme freeze-out conditions not recoverable with our angular resolution.

On the observational side, however, a rigorous comparison with previous results is challenging, since most of the estimates of  $f_D$ , whether derived from single-point spectra (e.g., [Thomas & Fuller 2008](#); [Fontani et al. 2012](#); [Giannetti et al. 2014](#)) or maps (e.g., [Hernandez et al. 2011](#); [Pon et al. 2016](#); [Feng et al. 2016a, 2020](#); [Sabatini et al. 2019](#) and [Gong et al. 2021](#)), are obtained at clump scale angular resolutions. Very few exceptions have been reported for high-mass star-forming regions (see [Zhang et al. 2009](#), [Morii et al. 2021](#) and [Rodríguez et al. 2021](#)). Within this context our results represent the first core-scale interferometric  $f_D$  maps observed with ALMA for a sample of high-mass clumps.

In the specific case of ASHES, [Morii et al. \(2021\)](#) estimated  $f_D$  using additional C<sup>18</sup>O(2-1) ASHES data observed in the 70  $\mu$ m dark IRDC G023.477+0.114. This source is not included in this work and in the pilot study published in [Sanhueza et al. \(2019\)](#). G023.477+0.114 has a near kinematic distance of  $5.2 \pm 0.5$  kpc, which implies a linear-scale resolution of  $\sim 5900$  au, comparable with those of the data presented in Sect. 2.1. The authors consider a variation of  $X_{C^{18}O}^E$  with the galactocentric distance of the source, and constant values for  $\gamma = 100$ . They report average  $f_D$  values between  $\sim 40$ –300 through the 11 cores at different evolutionary stages identified in G023.477+0.114. Notably, also in this case,  $f_D$  does not decrease going from the prestellar to the protostellar stage, and shows extreme values of  $f_D > 100$  associated with the most evolved sources, in agreement with our findings.

[Zhang et al. \(2009\)](#) conducted 1.3 mm spectral line and continuum observations of two massive molecular clumps harboured in the IRDC G28.34+0.06 ([Pillai et al. 2006](#) and [Wang et al. 2008](#)). The C<sup>18</sup>O(2-1) line was observed with the Submillimeter Array (SMA; [Ho et al. 2004](#)) telescope at a resolution of  $1.2''$  and with a final sensitivity of  $90 \text{ mJy beam}^{-1}$  at the spectral resolution of  $1.2 \text{ km s}^{-1}$ . These angular scale corresponds to  $\sim 4500$  au at the source heliocentric distance of 4.5 kpc ([Urquhart et al. 2018](#)), similar to the physical scales mapped in our ALMA observations. In each clump, the continuum dust emission at 1.3 mm has revealed multiple cores with typical sizes of  $\sim 5000$  au. However, out

of these cores only one shows a clear detection with an averaged value of  $f_D \sim 100$  ([Zhang et al. 2009](#)). The authors assumed  $\gamma = 100$  and  $X_{C^{18}O}^E = 5 \times 10^{-9}$ . If we rescale the  $f_D$  found for G28.34+0.06, assuming a galactocentric distance of 4.8 kpc in Equations (3) and (6)<sup>9</sup>, we obtain a  $f_D \sim 45$ , which is in line with the range of values reported in Fig. 3. Similarly, [Rodríguez et al. \(2021\)](#) observed the C<sup>18</sup>O(2-1) line toward the high-mass protostellar candidate ISOSS J23053+5953 SMM2 with SMA at  $\sim 2.5''$  ( $\sim 10^4$  au at the distance of 4.3 kpc). They report  $f_D \sim 20$ , already considering the variation of  $\gamma$  and  $X_{C^{18}O}^E$  with galactocentric distance of the source ( $\sim 10$  kpc [Bosco et al. 2019](#)).

It is worth noting that both the sources of [Zhang et al. \(2009\)](#) and [Rodríguez et al. \(2021\)](#) host mYSOs as demonstrated by the 24  $\mu$ m emission peaks and/or the presence of hot molecular cores with already developed outflows/jets. These high values observed in advanced evolutionary stages provide further evidence that on core scales, the degree of CO-depletion may not be suitable to follow the evolution of a core due to the huge amount of cold molecular gas that can surround a mYSO. These high densities could also increase the efficiency of dust grains coagulation ([Galamez et al. 2019](#)), implying a larger grain size and, in turn, decreasing the heating and subsequent evaporation of CO from the surface of the dust grains ([Iqbal & Wakelam 2018](#)).

Across the whole clump-scale, however, the revealed chemical picture changes. We have calculated the average  $f_D$  of each clump shown in Fig. 1 and 2, after convolving the  $N(\text{H}_2)$  and  $N(\text{C}^{18}\text{O})$  maps to an angular resolution equal to the effective radius of each clump (see Table 1). We associate with this derivation a conservative error of 15% that accounts for the fluctuations observed for  $f_D$  over the wide range of densities and temperatures found on the molecular cloud scale ([Sabatini et al. 2019](#)). We have correlated the average  $f_D$  of each source with the corresponding luminosity-to-mass ratio ( $L/M$ ) of the clumps, a well-known distance-independent evolutionary indicator for both low- and high-mass star-forming regions (e.g., [Saraceno et al. 1996](#); [Molinari et al. 2008](#) and [Urquhart et al. 2022](#)). The bolometric luminosity,  $L$ , and clump mass  $M$ , are taken from [Li et al. \(2020\)](#) with associated errors of 50% for  $L$  and 20% for  $M$ , respectively ([Urquhart et al. 2018](#)). These uncertainties have been derived from a statistical relevant sample of  $\sim 10^4$  high-mass clumps identified in

<sup>9</sup> Taking a brightness temperature of 2.5 K, a full width at half maximum (FWHM) of  $2.5 \text{ km s}^{-1}$ , a gas temperature of 30 K as reported by [Zhang et al. \(2009\)](#) for the detected C<sup>18</sup>O(2-1) line, and the derived a  $\gamma = 72$  and  $X_{C^{18}O}^E = 5.7 \times 10^{-7}$

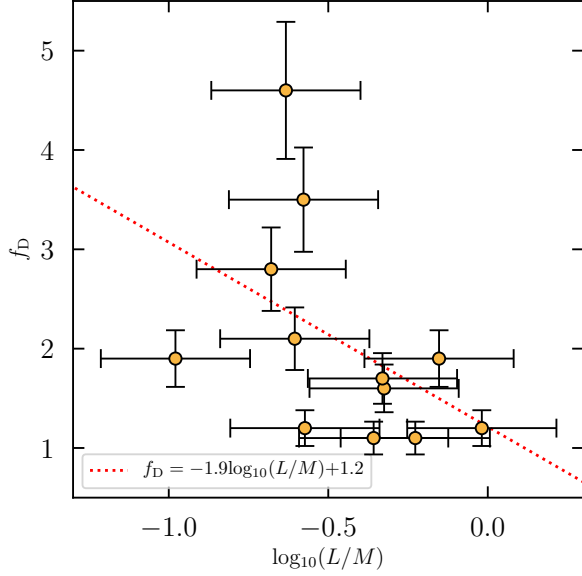


**Figure 6.** Correlation between  $f_D$  and the luminosity-to-mass ratio of the clumps that compose the ASHES sample. Yellow dots are associated with each source, while uncertainties are shown as black bars. Red dashed line represents the linear least-squares fit of  $f_D$  to the  $\log_{10}(L/M)$ . The fit parameters are shown in the legend, with Spearman’s rank correlation coefficient  $\rho_s = -0.62$  and a  $p$ -value = 0.03.

the APEX Telescope Large Area Survey of the Galaxy (Schuller et al. 2009).

Figure 6 shows the results of this correlation, presenting a clear downward trend of  $f_D$  with increasing  $L/M$ . A linear least-squares fit of  $f_D$  to the  $\log_{10}(L/M)$  is shown as a red-dashed line in the same figure. The averaged  $f_D$  is found to change by a factor of  $\sim 5$  for about one order of magnitude in  $L/M$ , yielding the power law relation  $f_D = -1.9 \log_{10}(L/M) + 1.2$ , with a Spearman’s rank correlation coefficient  $\rho_s = -0.62$  and a  $p$ -value = 0.03 (e.g., Zwillinger & Kokoska 1999; Cohen 2013). This result confirms the reliability of  $f_D$  to classify high-mass clumps at different evolutionary stages, as found in several samples, e.g., Fontani et al. (2012); Giannetti et al. (2014) and Sabatini et al. (2019). The different behaviour of  $f_D$  observed at clump and core-scale, might be the consequence of the complex interplay between chemistry and physics and their associated timescales. In particular, the chemical response to physical changes is smeared out when looking at clump scales, reflecting the average properties of the entire population of cores.

## 5. CONCLUSIONS

In this paper we presented the first core-scale  $f_D$  maps derived from  $C^{18}O(2-1)$  and 1.3 mm continuum ALMA

observations for the twelve 70  $\mu$ m-dark clumps of the ASHES sample. In this context, we have discussed whether the averaged CO-depletion factor computed at core scales can be considered a reliable evolutionary indicator of the high-mass star formation process.

The overall scenario that emerged from this study shows peculiar chemical conditions for the ISM involved in our targets, that changes according to the physical scale investigated. On the clump scale, we find that on average at least half of the expected CO has been removed from the gas phase, for more than 85% of the total area mapped in  $C^{18}O$ . The highest values of CO-depletion are found within the identified cores (both pre- and proto-stellar), where  $f_D$  values of more than 10 are reached in more than  $\sim 50\%$  of the cores.

In contrast to what has been observed for low-mass star-forming cores and, more generally, for high-mass clumps that have the potential to form high-mass stars, our analysis shows that the degree of the CO-depletion process on core-scales does not decrease during the transition from a prestellar to a protostellar phase. If we exclude the temperature effect due to the slight gradients in the  $T_{\text{kin}}^{\text{NH}_3}$  maps, we explain the evolutionary behaviour of  $f_D$  as primarily dependent on the average gas density, which increases with the evolution of the cores. This effect is not observed in the low-mass regime since the high-density regions have smaller sizes and are more affected by temperature variations driven by the star formation process. Furthermore, low-mass star-forming regions are also statistically closer to the Solar System, allowing for a better linear resolution. We emphasise that, due to the poorer resolution of the  $\text{NH}_3$  maps (on average a factor  $\sim 4$  coarser) compared to those of  $C^{18}O$ , temperature is also one of the main uncertainties affecting our results. Our analysis could greatly benefit from ammonia observations with a resolution comparable to that of ALMA. Nevertheless, we highlight the significant improvement for having derived temperatures at  $\sim 5''$  angular resolution with respect to adopting the Herschel dust temperatures at  $35''$  resolution.

The  $f_D$  fluctuations appear to be widely distributed when observed over thousands of astronomical units, and in particular trace the densest regions of clumps that are not always associated with a prestellar core. Our results lead us to classify  $f_D$  as a tracer that is not entirely reliable to distinguishing between prestellar and protostellar cores in a high-mass star-forming clumps. However, thanks to the high CO-depletion factors found in large parts of the clump, a more complete picture of evolution can be obtained by observing deuterated molecules. The abundance of ortho- $\text{H}_2\text{D}^+$ , for example, has been asserted as a clear chemical indi-

cator of prestellar stages both at the clump scale (e.g., Giannetti et al. 2019; Miettinen 2020 and Sabatini et al. 2020) and at the core-scales by the recent results of Redaelli et al. (2021) and Redaelli et al. (2022, *subm.*) obtained from ALMA data. Improving the sensitivity of astronomical facilities in the mm and sub-mm regime (such as APEX and ALMA) and the systematic study of deuterated molecules (such as  $\text{H}_2\text{D}^+$  and  $\text{D}_2\text{H}^+$ ) therefore seem to be the necessary breakthrough to finally obtain a comprehensive picture of the process of high-mass star formation.

The authors thank the anonymous Referee, for her/his suggestions to improve the manuscript. GS gratefully acknowledges financial support by the ANID BASAL project FB210003, and Dr R. Pascale for fruitful discussions. SB is financially supported by ANID Fondecyt Regular (project #1220033), and the ANID BASAL projects ACE210002 and FB210003. PS was partially supported by a Grant-in-Aid for Scientific Research (KAKENHI Number 18H01259 and 22H01271) of the Japan Society for the Promotion of Science (JSPS). KT was supported by JSPS KAKENHI (Grant Number 20H05645). This paper makes use of the ALMA data ADS/JAO.ALMA#2015.1.01539.S (PI: P. Sanhueza). ALMA is a partnership of ESO (representing its member states), NSF (USA) and NINS (Japan), together with NRC (Canada), MOST and ASIAA (Taiwan), and KASI (Republic of Korea), in cooperation with the Republic of Chile. The Joint ALMA Observatory is operated by ESO, AUI/NRAO and NAOJ.

*Facilities:* The Atacama Large Millimeter/submillimeter Array (ALMA; Wootten & Thompson 2009);

*Software:* This research has made use of `PySpecKit`, `ASTRODENDRO` (a Python package to compute dendrograms of Astronomical data), `APLpy` (an open-source plotting package for Python; Robitaille & Bressert 2012), `Astropy` (Astropy Collaboration et al. 2013, 2018), `NumPy` (Harris et al. 2020), `Matplotlib` (Hunter 2007), the Cologne Database for Molecular Spectroscopy (CDMS), and the NASA’s Astrophysics Data System Bibliographic Services (ADS);

## APPENDIX

### A. $\text{C}^{18}\text{O}$ OPACITY CORRECTION

When deriving the  $N(\text{C}^{18}\text{O})$ , it is worth inspecting whether the emission of  $\text{C}^{18}\text{O}(2-1)$  can be assumed optically thin. The optical depth of a transition can be estimated through the peak ratio of the same transition, coming from different isotopologues, if their relative abundance is known (e.g., Hofner et al. 2000). We computed  $\tau_{\text{C}^{18}\text{O}}$  using  $\text{C}^{17}\text{O}(2-1)$ ,  $\text{C}^{18}\text{O}(2-1)$  and  $\text{H}_2$  data published in Feng et al. 2020 observed in G014.492-00.139, and we refer to this paper for a more detailed description of the dataset. We selected this source since the final  $N(\text{H}_2)$  are among the highest of the entire ASHES sample, and therefore G014.492-00.139 represents a ideal case to study the variation of  $\tau_{\text{C}^{18}\text{O}}$ .

Assuming equal excitation temperatures and filling factor for the two species,  $\tau_{\text{C}^{18}\text{O}}$  is estimated as

$$R_{18,17} = \frac{T_{\text{mb}}^{\text{C}^{18}\text{O}}}{T_{\text{mb}}^{\text{C}^{17}\text{O}}} \propto \frac{[1 - \exp(-\tau_{\text{C}^{18}\text{O}})]}{[1 - \exp(-\tau_{\text{C}^{17}\text{O}})]}, \quad (\text{A1})$$

where,  $\tau_{\text{C}^{17}\text{O}}$  is the optical depth of  $\text{C}^{17}\text{O}(2-1)$  at  $\sim 224.7$  GHz, for which we assume  $\tau_{\text{C}^{17}\text{O}} = \tau_{\text{C}^{18}\text{O}}/4.16$  (e.g., Wouterloot et al. 2008). The fit is performed pixel-by-pixel for both  $\text{C}^{17}\text{O}$  and  $\text{C}^{18}\text{O}$  datacubes by taking data where both the continuum and the line emission have a  $>3\sigma$  level detection. We employ the Python Spectroscopic Toolkit (`PySpecKit`; Ginsburg & Mirocha 2011; Ginsburg et al. 2022), by using a single Gaussian component over a velocity space of  $\pm 3$  km s $^{-1}$  around the local standard of rest velocities ( $V_{\text{lsr}}$ ) derived in Sanhueza et al. (2019). The estimated  $\tau_{\text{C}^{18}\text{O}}$  are in the range of  $\sim 0.25$ - $1.80$ , implying optical depth correction factors  $C_\tau \in \{1.13 - 2.16\}$  to derive the final  $N(\text{C}^{18}\text{O})$

from Equation (4). In more than 75% of the sources detected in  $\text{C}^{18}\text{O}$ ,  $\tau_{\text{C}^{18}\text{O}} < 1.37$  ( $C_\tau < 1.84$ ). Similar  $\tau_{\text{C}^{18}\text{O}}$  are also reported in other Infrared Dark Cloud (e.g., Sanhueza et al. 2010; Sabatini et al. 2019; Gong et al. 2021), proving that  $\text{C}^{18}\text{O}$  is virtually always optically thin under the typical conditions prevalent in IRDCs.

To account for the same correction in the other ASHES sources, we follow the same approach of Sabatini et al. (2019), looking for a linear relation between  $\log_{10}(\tau_{\text{C}^{18}\text{O}})$  and  $\log_{10}[N(\text{H}_2)]$ . We have preferred the  $\text{H}_2$  column density over  $N(\text{C}^{18}\text{O})$  since  $N(\text{H}_2)$  is not affected by opacity at the observed size scales (i.e.,  $\kappa_\nu$  correction already applied in Sect. 3.1). The final  $\text{C}^{18}\text{O}$  column density maps are derived applying in each source the bestfit  $\log_{10}(\tau_{\text{C}^{18}\text{O}}) - \log_{10}[N(\text{H}_2)]$  relation obtained in G014.492-00.139, i.e.,  $\log_{10}(\tau_{\text{C}^{18}\text{O}}) = 0.6\log_{10}[N(\text{H}_2)] - 14.4$ .

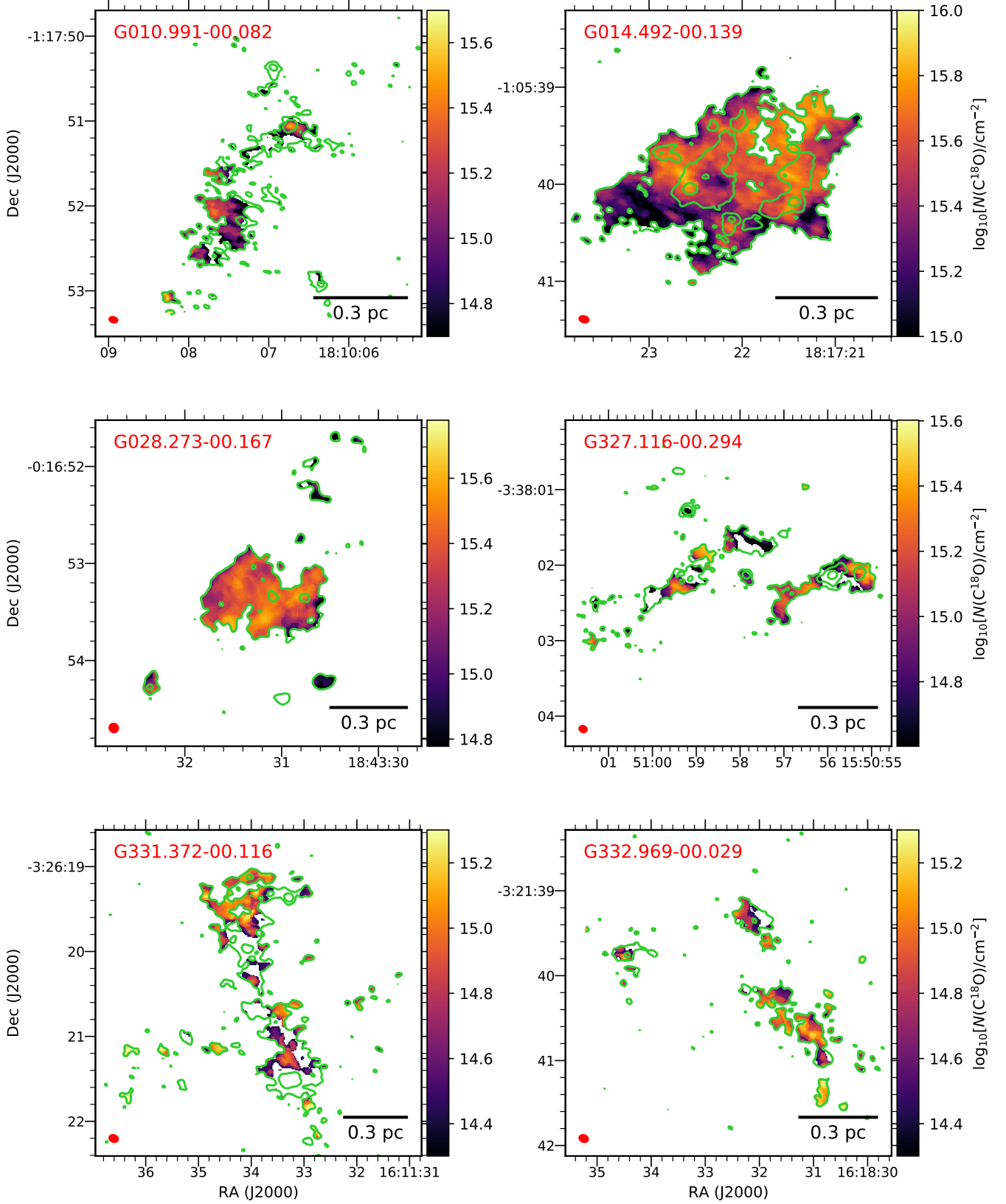
## B. NOTES ON THE ANALYSIS FOR INDIVIDUAL CLUMPS

The aim of this section is to test the influence of some specific properties of the clumps on the results discussed in the sections 3.3 and 4 (e.g., the heliocentric distance of the clumps, the number of cores, or the proportion of pre- and proto-stellar cores found in each ASHES source).

Figure 9 represents the analogue of Fig. 4, in which we have coloured the cores as a function of the heliocentric distance of the clumps hosting them. There is no clustering of cores when the distance of each source is considered, and the cores associated with each distance bin span comparable ranges of values in terms of  $f_D$  and  $n(\text{H}_2)$ , corresponding to at least a factor of  $\sim 5$ . Thus, the distribution of cores shown in Fig. 4 appears to be distance-independent, ruling out the influence of a possible distance bias on our results.

Figure 10 represents the analogue of Fig. 5, and shows the number distributions of the averaged  $f_D$  associated with ASHES cores within each clump, separately. Although the statistics of the cores in each clump is greatly reduced compared to the total number of cores shown in Fig. 5, we note that the median value of  $f_D$  derived for the prestellar population of cores (blue vertical lines in Fig. 10) is always lower than – or at most equal to – the value found for the protostellar cores (red dashed vertical lines; Figure 10). Figure 10 also shows that randomly removing a clump from the analysis presented in Sections 3.3 and 4 does not qualitatively change the general conclusions summarised in Sect. 5.





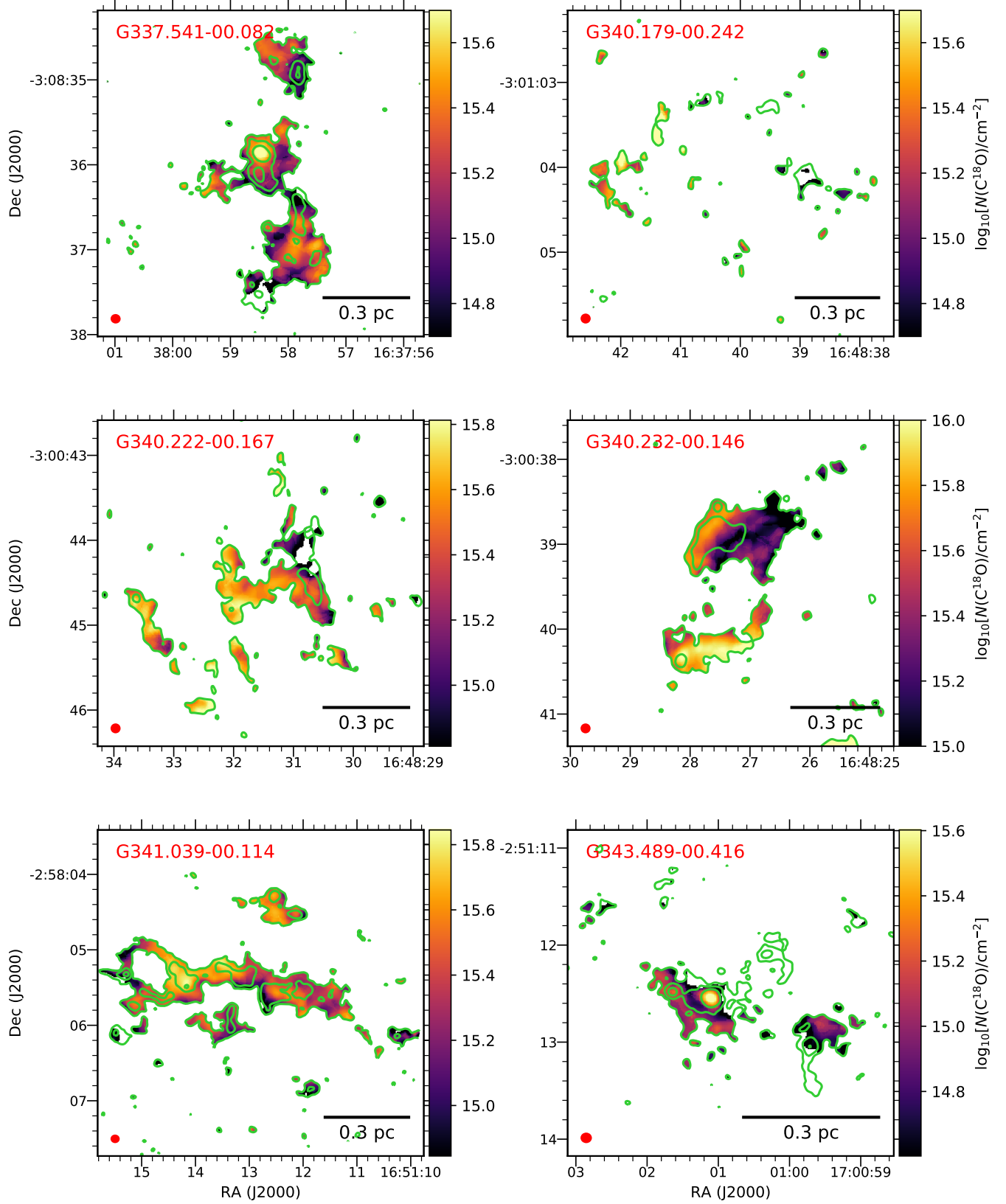
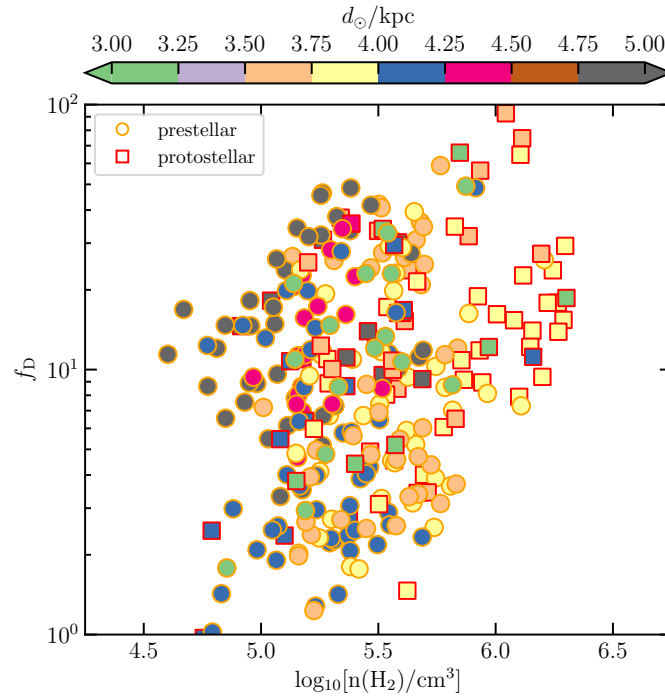


Figure 8. Continuation of Fig. 7.



**Figure 9.** Same as Figure 4(a) showing the variation in the average  $f_D$  and  $n(\text{H}_2)$  for the core population identified in ASHES as a function of the heliocentric distance of each clump (indicated in the colour wedge; see also Tab. 1). Circles and squares represent the prestellar and protostellar cores, respectively.

## REFERENCES

- Adams, F. C. 2010, *ARA&A*, 48, 47,  
doi: [10.1146/annurev-astro-081309-130830](https://doi.org/10.1146/annurev-astro-081309-130830)
- Allingham, D., . et al., 2022 in prep.
- Astropy Collaboration, Robitaille, T. P., Tollerud, E. J.,  
et al. 2013, *A&A*, 558, A33,  
doi: [10.1051/0004-6361/201322068](https://doi.org/10.1051/0004-6361/201322068)
- Astropy Collaboration, Price-Whelan, A. M., Sipőcz, B. M.,  
et al. 2018, *AJ*, 156, 123, doi: [10.3847/1538-3881/aabc4f](https://doi.org/10.3847/1538-3881/aabc4f)
- Battersby, C., Bally, J., Jackson, J. M., et al. 2010, *ApJ*,  
721, 222, doi: [10.1088/0004-637X/721/1/222](https://doi.org/10.1088/0004-637X/721/1/222)
- Bergin, E. A., Alves, J., Huard, T., & Lada, C. J. 2002,  
*ApJL*, 570, L101, doi: [10.1086/340950](https://doi.org/10.1086/340950)
- Bonnell, I. A., Bate, M. R., Clarke, C. J., & Pringle, J. E.  
2001, *MNRAS*, 323, 785,  
doi: [10.1046/j.1365-8711.2001.04270.x](https://doi.org/10.1046/j.1365-8711.2001.04270.x)
- Bosco, F., Beuther, H., Ahmadi, A., et al. 2019, *A&A*, 629,  
A10, doi: [10.1051/0004-6361/201935318](https://doi.org/10.1051/0004-6361/201935318)
- Bovino, S., Ferrada-Chamorro, S., Lupi, A., et al. 2019,  
*ApJ*, 887, 224, doi: [10.3847/1538-4357/ab53e4](https://doi.org/10.3847/1538-4357/ab53e4)
- Carey, S. J., Clark, F. O., Egan, M. P., et al. 1998, *ApJ*,  
508, 721, doi: [10.1086/306438](https://doi.org/10.1086/306438)
- Carey, S. J., Noriega-Crespo, A., Mizuno, D. R., et al.  
2009, *PASP*, 121, 76, doi: [10.1086/596581](https://doi.org/10.1086/596581)
- Caselli, P., Vastel, C., Ceccarelli, C., et al. 2008, *A&A*, 492,  
703, doi: [10.1051/0004-6361:20079009](https://doi.org/10.1051/0004-6361:20079009)
- Caselli, P., Walmsley, C. M., Tafalla, M., Dore, L., &  
Myers, P. C. 1999, *ApJL*, 523, L165, doi: [10.1086/312280](https://doi.org/10.1086/312280)
- Cesaroni, R. 2005, in *IAU Symposium*, Vol. 227, *Massive  
Star Birth: A Crossroads of Astrophysics*, ed.  
R. Cesaroni, M. Felli, E. Churchwell, & M. Walmsley,  
59–69, doi: [10.1017/S1743921305004369](https://doi.org/10.1017/S1743921305004369)
- Chambers, E. T., Jackson, J. M., Rathborne, J. M., &  
Simon, R. 2009, *ApJS*, 181, 360,  
doi: [10.1088/0067-0049/181/2/360](https://doi.org/10.1088/0067-0049/181/2/360)
- Cohen, J. 2013, *Statistical power analysis for the behavioral  
sciences* (Routledge)
- Contreras, Y., Rathborne, J. M., Guzman, A., et al. 2017,  
*MNRAS*, 466, 340, doi: [10.1093/mnras/stw3110](https://doi.org/10.1093/mnras/stw3110)
- Contreras, Y., Sanhueza, P., Jackson, J. M., et al. 2018,  
*ApJ*, 861, 14, doi: [10.3847/1538-4357/aac2ec](https://doi.org/10.3847/1538-4357/aac2ec)
- Egan, M. P., Shipman, R. F., Price, S. D., et al. 1998,  
*ApJL*, 494, L199, doi: [10.1086/311198](https://doi.org/10.1086/311198)
- Elia, D., Molinari, S., Schisano, E., et al. 2017, *MNRAS*,  
471, 100, doi: [10.1093/mnras/stx1357](https://doi.org/10.1093/mnras/stx1357)
- Elia, D., Merello, M., Molinari, S., et al. 2021, *MNRAS*,  
504, 2742, doi: [10.1093/mnras/stab1038](https://doi.org/10.1093/mnras/stab1038)

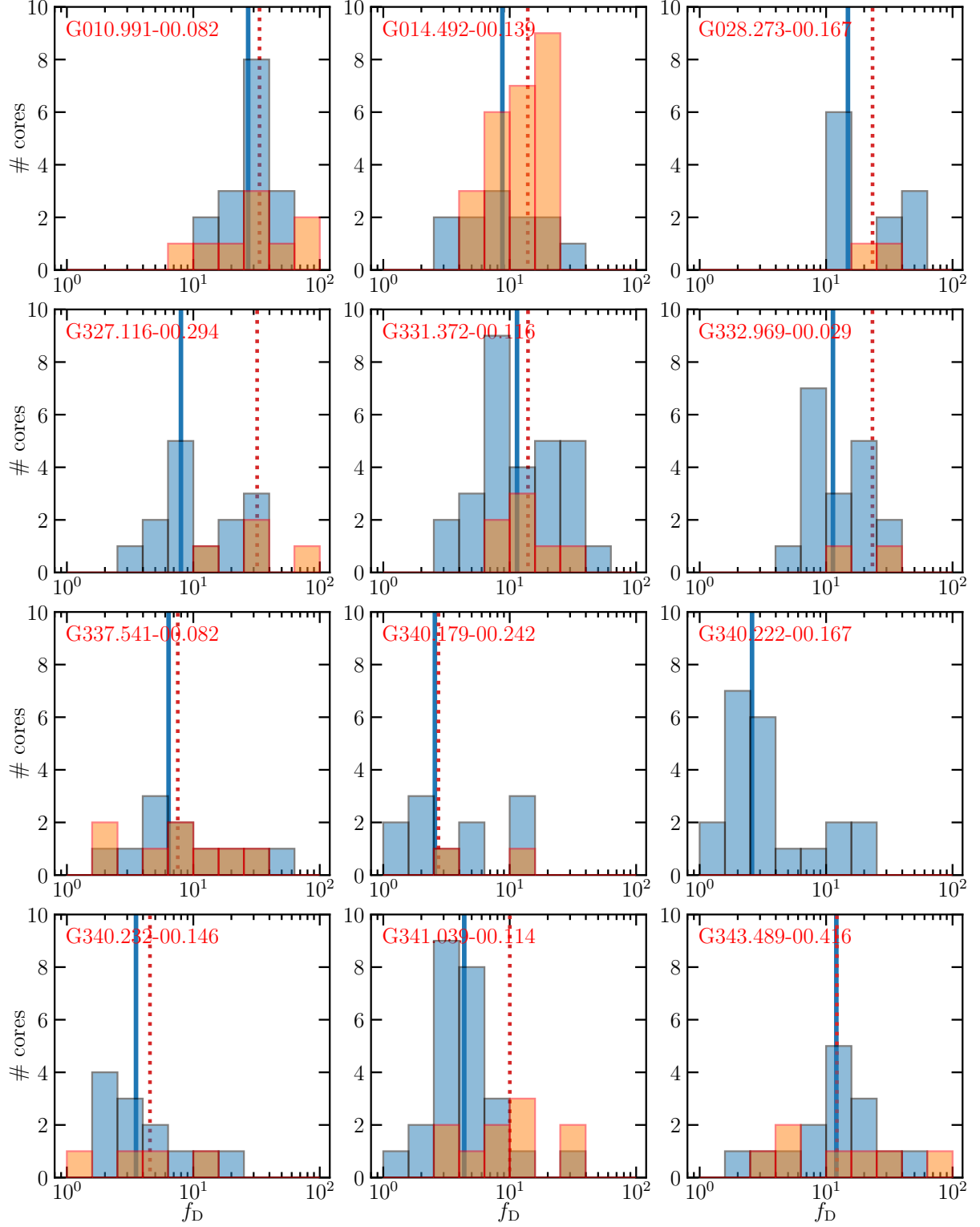


**Figure 10.** Same as Figure 5 showing the number distributions of the averaged  $f_D$  associated with each core identified in ASHES. In the different panels, the distributions within each clump are shown separately (red labels in the upper left corners). The blue and orange histograms refer to prestellar and protostellar cores, respectively. The vertical lines represent the median of  $f_D$  resulting from the distributions of prestellar (blue lines) and protostellar (red-dashed lines) cores.

- Elmegreen, B. G. 1998, in *Astronomical Society of the Pacific Conference Series*, Vol. 148, *Origins*, ed. C. E. Woodward, J. M. Shull, & J. Thronson, Harley A., 150. <https://arxiv.org/abs/astro-ph/9712352>
- Feng, S., Beuther, H., Zhang, Q., et al. 2016a, *A&A*, 592, A21, doi: [10.1051/0004-6361/201526864](https://doi.org/10.1051/0004-6361/201526864)
- . 2016b, *ApJ*, 828, 100, doi: [10.3847/0004-637X/828/2/100](https://doi.org/10.3847/0004-637X/828/2/100)
- Feng, S., Li, D., Caselli, P., et al. 2020, *ApJ*, 901, 145, doi: [10.3847/1538-4357/abada3](https://doi.org/10.3847/1538-4357/abada3)
- Fontani, F., Caselli, P., Crapsi, A., et al. 2006, *A&A*, 460, 709, doi: [10.1051/0004-6361:20066105](https://doi.org/10.1051/0004-6361:20066105)
- Fontani, F., Giannetti, A., Beltrán, M. T., et al. 2012, *MNRAS*, 423, 2342, doi: [10.1111/j.1365-2966.2012.21043.x](https://doi.org/10.1111/j.1365-2966.2012.21043.x)
- Frerking, M. A., Langer, W. D., & Wilson, R. W. 1982, *ApJ*, 262, 590, doi: [10.1086/160451](https://doi.org/10.1086/160451)
- Friesen, R. K., Di Francesco, J., Shirley, Y. L., & Myers, P. C. 2009, *ApJ*, 697, 1457, doi: [10.1088/0004-637X/697/2/1457](https://doi.org/10.1088/0004-637X/697/2/1457)
- Galametz, M., Maury, A. J., Valdivia, V., et al. 2019, *A&A*, 632, A5, doi: [10.1051/0004-6361/201936342](https://doi.org/10.1051/0004-6361/201936342)
- Giannetti, A., Leurini, S., Wyrowski, F., et al. 2017a, *A&A*, 603, A33, doi: [10.1051/0004-6361/201630048](https://doi.org/10.1051/0004-6361/201630048)
- Giannetti, A., Wyrowski, F., Brand, J., et al. 2014, *A&A*, 570, A65, doi: [10.1051/0004-6361/201423692](https://doi.org/10.1051/0004-6361/201423692)
- Giannetti, A., Leurini, S., König, C., et al. 2017b, *A&A*, 606, L12, doi: [10.1051/0004-6361/201731728](https://doi.org/10.1051/0004-6361/201731728)
- Giannetti, A., Bovino, S., Caselli, P., et al. 2019, *A&A*, 621, L7, doi: [10.1051/0004-6361/201834602](https://doi.org/10.1051/0004-6361/201834602)
- Ginsburg, A., & Mirocha, J. 2011, *PySpecKit: Python Spectroscopic Toolkit*. <http://ascl.net/1109.001>
- Ginsburg, A., Sokolov, V., de Val-Borro, M., et al. 2022, *AJ*, 163, 291, doi: [10.3847/1538-3881/ac695a](https://doi.org/10.3847/1538-3881/ac695a)
- Goldsmith, P. F. 2001, *ApJ*, 557, 736, doi: [10.1086/322255](https://doi.org/10.1086/322255)
- Gong, Y., Belloche, A., Du, F. J., et al. 2021, *A&A*, 646, A170, doi: [10.1051/0004-6361/202039465](https://doi.org/10.1051/0004-6361/202039465)
- Güsten, R., Nyman, L. Å., Schilke, P., et al. 2006, *A&A*, 454, L13, doi: [10.1051/0004-6361:20065420](https://doi.org/10.1051/0004-6361:20065420)
- Guzmán, A. E., Sanhueza, P., Contreras, Y., et al. 2015, *ApJ*, 815, 130, doi: [10.1088/0004-637X/815/2/130](https://doi.org/10.1088/0004-637X/815/2/130)
- Harris, C. R., Millman, K. J., van der Walt, S. J., et al. 2020, *Nature*, 585, 357, doi: [10.1038/s41586-020-2649-2](https://doi.org/10.1038/s41586-020-2649-2)
- Herbst, E., & van Dishoeck, E. F. 2009, *ARA&A*, 47, 427, doi: [10.1146/annurev-astro-082708-101654](https://doi.org/10.1146/annurev-astro-082708-101654)
- Hernandez, A. K., Tan, J. C., Caselli, P., et al. 2011, *ApJ*, 738, 11, doi: [10.1088/0004-637X/738/1/11](https://doi.org/10.1088/0004-637X/738/1/11)
- Herzberg, G. 1945, *Molecular spectra and molecular structure. Vol.2: Infrared and Raman spectra of polyatomic molecules*
- Heyer, M., & Dame, T. M. 2015, *ARA&A*, 53, 583, doi: [10.1146/annurev-astro-082214-122324](https://doi.org/10.1146/annurev-astro-082214-122324)
- Ho, P. T. P., Moran, J. M., & Lo, K. Y. 2004, *ApJ*, 616, L1, doi: [10.1086/423245](https://doi.org/10.1086/423245)
- Hoare, M. G., Purcell, C. R., Churchwell, E. B., et al. 2012, *PASP*, 124, 939, doi: [10.1086/668058](https://doi.org/10.1086/668058)
- Hofner, P., Wyrowski, F., Walmsley, C. M., & Churchwell, E. 2000, *ApJ*, 536, 393, doi: [10.1086/308903](https://doi.org/10.1086/308903)
- Hogge, T., Jackson, J., Stephens, I., et al. 2018, *ApJS*, 237, 27, doi: [10.3847/1538-4365/aac9f4](https://doi.org/10.3847/1538-4365/aac9f4)
- Hunter, J. D. 2007, *Computing In Science & Engineering*, 9, 90, doi: [10.1109/MCSE.2007.55](https://doi.org/10.1109/MCSE.2007.55)
- Iguchi, S., Morita, K.-I., Sugimoto, M., et al. 2009, *PASJ*, 61, 1, doi: [10.1093/pasj/61.1.1](https://doi.org/10.1093/pasj/61.1.1)
- Iqbal, W., & Wakelam, V. 2018, *A&A*, 615, A20, doi: [10.1051/0004-6361/201732486](https://doi.org/10.1051/0004-6361/201732486)
- Kauffmann, J., Bertoldi, F., Bourke, T. L., Evans, N. J., I., & Lee, C. W. 2008, *A&A*, 487, 993, doi: [10.1051/0004-6361:200809481](https://doi.org/10.1051/0004-6361:200809481)
- Keown, J., Di Francesco, J., Rosolowsky, E., et al. 2019, *ApJ*, 884, 4, doi: [10.3847/1538-4357/ab3e76](https://doi.org/10.3847/1538-4357/ab3e76)
- König, C., Urquhart, J. S., Csengeri, T., et al. 2017, *A&A*, 599, A139, doi: [10.1051/0004-6361/201526841](https://doi.org/10.1051/0004-6361/201526841)
- Kramer, C., Alves, J., Lada, C. J., et al. 1999, *A&A*, 342, 257
- Kramer, C., & Winnewisser, G. 1991, *Astronomy and Astrophysics Supplement Series*, 89, 421
- Kumar, M. S. N., Palmeirim, P., Arzoumanian, D., & Inutsuka, S. I. 2020, *A&A*, 642, A87, doi: [10.1051/0004-6361/202038232](https://doi.org/10.1051/0004-6361/202038232)
- Kurtz, S., Cesaroni, R., Churchwell, E., Hofner, P., & Walmsley, C. M. 2000, in *Protostars and Planets IV*, ed. V. Mannings, A. P. Boss, & S. S. Russell, 299–326
- Li, Shanghuo, . et al., 2022 in prep.
- Li, S., Zhang, Q., Pillai, T., et al. 2019, *ApJ*, 886, 130, doi: [10.3847/1538-4357/ab464e](https://doi.org/10.3847/1538-4357/ab464e)
- Li, S., Sanhueza, P., Zhang, Q., et al. 2020, *ApJ*, 903, 119, doi: [10.3847/1538-4357/abb81f](https://doi.org/10.3847/1538-4357/abb81f)
- Li, S., Sanhueza, P., Lee, C. W., et al. 2022, *ApJ*, 926, 165, doi: [10.3847/1538-4357/ac3df8](https://doi.org/10.3847/1538-4357/ac3df8)
- Luck, R. E., & Lambert, D. L. 2011, *AJ*, 142, 136, doi: [10.1088/0004-6256/142/4/136](https://doi.org/10.1088/0004-6256/142/4/136)
- Mangum, J. G., & Shirley, Y. L. 2015, *PASP*, 127, 266, doi: [10.1086/680323](https://doi.org/10.1086/680323)
- Massey, F. J. 1951, *Journal of the American Statistical Association*, 46, 68, doi: [10.1080/01621459.1951.10500769](https://doi.org/10.1080/01621459.1951.10500769)
- McKee, C. F., & Tan, J. C. 2002, *Nature*, 416, 59, doi: [10.1038/416059a](https://doi.org/10.1038/416059a)
- Miettinen, O. 2020, *A&A*, 634, A115, doi: [10.1051/0004-6361/201936730](https://doi.org/10.1051/0004-6361/201936730)



- Molinari, S., Pezzuto, S., Cesaroni, R., et al. 2008, *A&A*, 481, 345, doi: [10.1051/0004-6361:20078661](https://doi.org/10.1051/0004-6361:20078661)
- Molinari, S., Swinyard, B., Bally, J., et al. 2010, *PASP*, 122, 314, doi: [10.1086/651314](https://doi.org/10.1086/651314)
- Morii, K., Sanhueza, P., Nakamura, F., et al. 2021, *ApJ*, 923, 147, doi: [10.3847/1538-4357/ac2365](https://doi.org/10.3847/1538-4357/ac2365)
- Müller, H. S. P., Thorwirth, S., Roth, D. A., & Winnewisser, G. 2001, *A&A*, 370, L49, doi: [10.1051/0004-6361:20010367](https://doi.org/10.1051/0004-6361:20010367)
- Ossenkopf, V., & Henning, T. 1994, *A&A*, 291, 943
- Padoan, P., Pan, L., Juvela, M., Haugbølle, T., & Nordlund, Å. 2020, *ApJ*, 900, 82, doi: [10.3847/1538-4357/abaa47](https://doi.org/10.3847/1538-4357/abaa47)
- Perault, M., Omont, A., Simon, G., et al. 1996, *A&A*, 315, L165
- Peretto, N., Lenfestey, C., Fuller, G. A., et al. 2016, *A&A*, 590, A72, doi: [10.1051/0004-6361/201527064](https://doi.org/10.1051/0004-6361/201527064)
- Pilbratt, G. L., Riedinger, J. R., Passvogel, T., et al. 2010, *A&A*, 518, L1, doi: [10.1051/0004-6361/201014759](https://doi.org/10.1051/0004-6361/201014759)
- Pillai, T., Wyrowski, F., Carey, S. J., & Menten, K. M. 2006, *A&A*, 450, 569, doi: [10.1051/0004-6361:20054128](https://doi.org/10.1051/0004-6361:20054128)
- Pillai, T., Wyrowski, F., Hatchell, J., Gibb, A. G., & Thompson, M. A. 2007, *A&A*, 467, 207, doi: [10.1051/0004-6361:20065682](https://doi.org/10.1051/0004-6361:20065682)
- Pokhrel, R., Myers, P. C., Dunham, M. M., et al. 2018, *ApJ*, 853, 5, doi: [10.3847/1538-4357/aaa240](https://doi.org/10.3847/1538-4357/aaa240)
- Pon, A., Johnstone, D., Caselli, P., et al. 2016, *A&A*, 587, A96, doi: [10.1051/0004-6361/201527154](https://doi.org/10.1051/0004-6361/201527154)
- Price, S. D., Egan, M. P., Carey, S. J., Mizuno, D. R., & Kuchar, T. A. 2001, *AJ*, 121, 2819, doi: [10.1086/320404](https://doi.org/10.1086/320404)
- Rathborne, J. M., Jackson, J. M., & Simon, R. 2006, *ApJ*, 641, 389, doi: [10.1086/500423](https://doi.org/10.1086/500423)
- Redaelli, E., Bovino, S., Giannetti, A., et al. 2021, *A&A*, 650, A202, doi: [10.1051/0004-6361/202140694](https://doi.org/10.1051/0004-6361/202140694)
- Redaelli, E., Bovino, S., Sanhueza, P., et al. 2022, *subm.*
- Reid, M. J., Menten, K. M., Brunthaler, A., et al. 2014, *ApJ*, 783, 130, doi: [10.1088/0004-637X/783/2/130](https://doi.org/10.1088/0004-637X/783/2/130)
- Rieke, G. H., Young, E. T., Engelbracht, C. W., et al. 2004, *ApJS*, 154, 25, doi: [10.1086/422717](https://doi.org/10.1086/422717)
- Robitaille, T., & Bressert, E. 2012, *APLpy: Astronomical Plotting Library in Python*, Astrophysics Source Code Library, record ascl:1208.017. <http://ascl.net/1208.017>
- Rodríguez, T. M., Hofner, P., Araya, E. D., et al. 2021, *ApJ*, 922, 66, doi: [10.3847/1538-4357/ac2366](https://doi.org/10.3847/1538-4357/ac2366)
- Sabatini, G., Giannetti, A., Bovino, S., et al. 2019, *MNRAS*, 490, 4489, doi: [10.1093/mnras/stz2818](https://doi.org/10.1093/mnras/stz2818)
- Sabatini, G., Bovino, S., Giannetti, A., et al. 2020, *A&A*, 644, A34, doi: [10.1051/0004-6361/202039010](https://doi.org/10.1051/0004-6361/202039010)
- . 2021, *A&A*, 652, A71, doi: [10.1051/0004-6361/202140469](https://doi.org/10.1051/0004-6361/202140469)
- Sakai, T., Sanhueza, P., Furuya, K., et al. 2022, *ApJ*, 925, 144, doi: [10.3847/1538-4357/ac3d2e](https://doi.org/10.3847/1538-4357/ac3d2e)
- Sanhueza, P., Garay, G., Bronfman, L., et al. 2010, *ApJ*, 715, 18, doi: [10.1088/0004-637X/715/1/18](https://doi.org/10.1088/0004-637X/715/1/18)
- Sanhueza, P., Jackson, J. M., Foster, J. B., et al. 2012, *ApJ*, 756, 60, doi: [10.1088/0004-637X/756/1/60](https://doi.org/10.1088/0004-637X/756/1/60)
- . 2013, *ApJ*, 773, 123, doi: [10.1088/0004-637X/773/2/123](https://doi.org/10.1088/0004-637X/773/2/123)
- Sanhueza, P., Jackson, J. M., Zhang, Q., et al. 2017, *The Astrophysical Journal*, 841, 97, doi: [10.3847/1538-4357/aa6ff8](https://doi.org/10.3847/1538-4357/aa6ff8)
- Sanhueza, P., Contreras, Y., Wu, B., et al. 2019, *ApJ*, 886, 102, doi: [10.3847/1538-4357/ab45e9](https://doi.org/10.3847/1538-4357/ab45e9)
- Saraceno, P., Andre, P., Ceccarelli, C., Griffin, M., & Molinari, S. 1996, *A&A*, 309, 827
- Schuller, F., Menten, K. M., Contreras, Y., et al. 2009, *A&A*, 504, 415, doi: [10.1051/0004-6361/200811568](https://doi.org/10.1051/0004-6361/200811568)
- Simon, R., Jackson, J. M., Rathborne, J. M., & Chambers, E. T. 2006a, *ApJ*, 639, 227, doi: [10.1086/499342](https://doi.org/10.1086/499342)
- Simon, R., Rathborne, J. M., Shah, R. Y., Jackson, J. M., & Chambers, E. T. 2006b, *ApJ*, 653, 1325, doi: [10.1086/508915](https://doi.org/10.1086/508915)
- Tafuya, D., Sanhueza, P., Zhang, Q., et al. 2021, *ApJ*, 913, 131, doi: [10.3847/1538-4357/abf5da](https://doi.org/10.3847/1538-4357/abf5da)
- Teegavarapu, R. S. 2019, in *Trends and Changes in Hydroclimatic Variables*, ed. R. Teegavarapu (Elsevier), 1–89, doi: [10.1016/B978-0-12-810985-4.00001-3](https://doi.org/10.1016/B978-0-12-810985-4.00001-3)
- Thomas, H. S., & Fuller, G. A. 2008, *A&A*, 479, 751, doi: [10.1051/0004-6361:20066499](https://doi.org/10.1051/0004-6361:20066499)
- Tigé, J., Motte, F., Russeil, D., et al. 2017, *A&A*, 602, A77, doi: [10.1051/0004-6361/201628989](https://doi.org/10.1051/0004-6361/201628989)
- Urquhart, J. S., Hoare, M. G., Purcell, C. R., et al. 2009, *A&A*, 501, 539, doi: [10.1051/0004-6361/200912108](https://doi.org/10.1051/0004-6361/200912108)
- Urquhart, J. S., König, C., Giannetti, A., et al. 2018, *MNRAS*, 473, 1059, doi: [10.1093/mnras/stx2258](https://doi.org/10.1093/mnras/stx2258)
- Urquhart, J. S., Wells, M. R. A., Pillai, T., et al. 2022, *MNRAS*, 510, 3389, doi: [10.1093/mnras/stab3511](https://doi.org/10.1093/mnras/stab3511)
- Wang, K., Zhang, Q., Testi, L., et al. 2014, *MNRAS*, 439, 3275, doi: [10.1093/mnras/stu127](https://doi.org/10.1093/mnras/stu127)
- Wang, Y., Zhang, Q., Pillai, T., Wyrowski, F., & Wu, Y. 2008, *ApJL*, 672, L33, doi: [10.1086/524949](https://doi.org/10.1086/524949)
- Whitaker, J. S., Jackson, J. M., Rathborne, J. M., et al. 2017, *AJ*, 154, 140, doi: [10.3847/1538-3881/aa86ad](https://doi.org/10.3847/1538-3881/aa86ad)
- Wiles, B., Lo, N., Redman, M. P., et al. 2016, *MNRAS*, 458, 3429, doi: [10.1093/mnras/stw525](https://doi.org/10.1093/mnras/stw525)
- Wilson, T. L., & Rood, R. 1994, *ARA&A*, 32, 191, doi: [10.1146/annurev.aa.32.090194.001203](https://doi.org/10.1146/annurev.aa.32.090194.001203)
- Wilson, W. E., Ferris, R. H., Axtens, P., et al. 2011, *MNRAS*, 416, 832, doi: [10.1111/j.1365-2966.2011.19054.x](https://doi.org/10.1111/j.1365-2966.2011.19054.x)
- Wootten, A., & Thompson, A. R. 2009, *IEEE Proceedings*, 97, 1463, doi: [10.1109/JPROC.2009.2020572](https://doi.org/10.1109/JPROC.2009.2020572)

- Wouterloot, J. G. A., Henkel, C., Brand, J., & Davis, G. R. 2008, A&A, 487, 237, doi: [10.1051/0004-6361:20078156](https://doi.org/10.1051/0004-6361:20078156)
- Zhang, Q., & Wang, K. 2011, ApJ, 733, 26, doi: [10.1088/0004-637X/733/1/26](https://doi.org/10.1088/0004-637X/733/1/26)
- Zhang, Q., Wang, Y., Pillai, T., & Rathborne, J. 2009, ApJ, 696, 268, doi: [10.1088/0004-637X/696/1/268](https://doi.org/10.1088/0004-637X/696/1/268)
- Zhang, Y., Tan, J. C., & Hosokawa, T. 2014, ApJ, 788, 166, doi: [10.1088/0004-637X/788/2/166](https://doi.org/10.1088/0004-637X/788/2/166)
- Zwillinger, D., & Kokoska, S. 1999, CRC standard probability and statistics tables and formulae (Crc Press)